Order Number 8820843

The effects of bandwidth on the detection of narrow- and wide-band auditory signals

Bernstein, Richard Saul, Ph.D.

City University of New York, 1988

U·M·I
300 N. Zeeb Rd.
Ann Arbor, MI 48106

PLEASE NOTE:

In all cases this material has been filmed in the best possible way from the available copy. Problems encountered with this document have been identified here with a check mark __✓__.

1. Glossy photographs or pages _____
2. Colored illustrations, paper or print _____
3. Photographs with dark background _____
4. Illustrations are poor copy _____
5. Pages with black marks, not original copy _____
6. Print shows through as there is text on both sides of page _____
7. Indistinct, broken or small print on several pages ✓
8. Print exceeds margin requirements _____
9. Tightly bound copy with print lost in spine _____
10. Computer printout pages with indistinct print _____
11. Page(s) _____ lacking when material received, and not available from school or author.
12. Page(s) _____ seem to be missing in numbering only as text follows.
13. Two pages numbered _____. Text follows.
14. Curling and wrinkled pages _____
15. Dissertation contains pages with print at a slant, filmed as received _____
16. Other _____

_____

_____

The Effects of Bandwidth on the Detection of Narrow- and Wide-Band Auditory Signals

by

Richard S. Bernstein

A dissertation submitted to the Graduate Faculty in Psychology in partial fulfillment of the requirements for the degree of Doctor of Philosophy, The City University of New York.

1988

This manuscript has been read and accepted for the Graduate Faculty in Psychology in satisfaction of the dissertation requirement for the degree of Doctor of Philosophy.

1-29-88
Date

David H. Raab
Chair of Examining Committee

January 29, 1988
Date

Herbert S. Saltzstein
Executive Officer

Dr. Gerard Bruder

Dr. Eric Heinemann

Dr. Neil Macmillan

Dr. Eli Osman

Dr. David Raab

Supervisory Committee

The City University of New York

Abstract

The Effects of Bandwidth on the Detection of Narrow- and Wide-Band Auditory Signals

by

Richard S. Bernstein

Advisor: Professor David H. Raab

Since Fletcher's classic paper on auditory masking, theorists have usually assumed that listeners base their decisions about the presence of a signal on some internal representation of stimulus energy and that critical bandwidths represent limits of integration. An energy-detection model (without internal filtering) predicts that threshold should increase with masker bandwidth at a rate of approximately 5 dB per decade increase in masker bandwidth. Empirical estimates of this rate are usually larger than this theoretical value.

The model also predicts that threshold will vary inversely with the bandwidth of a noise signal. The predicted rate depends on the relationship between signal and masker bandwidths. Although rate has been shown to depend on whether masker bandwidth equals or exceeds signal bandwidth, the details of this dependency have not been established. From these considerations, it seemed worthwhile to study the detectability of signals with bandwidths that are sub-critical ("narrow") and supra-critical ("wide") in the presence of maskers of various bandwidths. Since predictions depend on specifications of bandwidth synthetic noises with nearly rectangular spectra were

employed.

For both narrow- and wide-band signals, increasing masker bandwidth resulted in elevation of signal threshold until some *critical* bandwidth was exceeded. Thresholds of narrow-band signals increased at the rate of 8 dB per decade increase in masker bandwidth, whereas thresholds of wide-band signals increased at a rate of 25 dB. These *critical* bandwidths were found to vary with signal bandwidth suggesting that listeners adjust the bandwidth of the detection process in accord with the spectrum of the signal.

Threshold was found to vary inversely with signal bandwidth. When signal and masker had the same bandlimits, threshold improved at the rate of 3 dB per decade increase in bandwidth. On the other hand, and for all signals, when masker bandwidth exceeded the signal's *critical* width, threshold improved at the rate of 7 dB. Rate was found to be a function of the difference between masker and signal bandwidths.

The addition of a bandwidth-dependent variance term to an energy-detection model was found to improve the ability of the model to predict thresholds of narrow-band signals. This variance is due to internal processing. The modified model also predicted the effect of signal bandwidth on threshold. However, the effect of masker bandwidth on thresholds of wide-band signals was greater than predicted. From these findings, it is argued -- in agreement with others -- that detection is based on internal representations of stimulus energy. Processing imposes bandwidth-dependent variability on the internal representation. An additional mechanism becomes important with wide-band signals: The *spectral contours* of these signals are enhanced by a operation whichs adjusts the gain of each critical band.

This dissertation is dedicated to my wife, Donna, for her love and patience and is also dedicated to my family for their support.

Thanks are due to many faculty members of several departments for their help and guidance. I am especially indebted to Dr. Raab for being my mentor. Computer facilities were provided by the Computer Center of the City University of New York and by the Department of Psychology at Brooklyn College.

Table of Contents

1.	INTRODUCTION	1
1.1	Detection of Tones Masked by Noise	1
1.1.1	The Power-Spectrum Model	1
1.1.2	The Energy-Detection Model	6
1.1.3	The Effect of Internal Filtering on Fletcher Plots	11
1.2	Detection of Noise Signals Masked by Noise	14
1.2.1	Power-Spectrum Model	14
1.2.2	Energy-Detection Model	16
1.3	Summary	16
2.	METHODS	17
2.1	Subjects	17
2.2	Apparatus	17
2.3	Procedures	21
2.3.1	Psychophysical Method	21
2.3.2	Experimental Design	23
3.	RESULTS	25
3.1	Sub-Critical Bandwidth Signals	25
3.1.1	Detectability as a Function of Masker Bandwidth	25
3.1.2	Effect of Masker Level	30
3.1.3	Comparison of the Masking of the Tone and Narrow-Band Noise Signals	30

3.2	Supra-Critical Bandwidth Signals	40
3.2.1	Effect of Masker Bandwidth	40
3.2.2	Effect of Masker Level	40
3.2.3	Effect of Signal Bandwidth	49
3.3	Summary	60
4.	DISCUSSION	61
4.1	Detection of Narrow-Band Signals	61
4.1.1	Tonal Signals	61
4.1.2	Narrow-Band Noise Signal	74
4.2	Detection of Wide-Band Signals	76
4.2.1	The Fletcher Plot	76
4.2.1	Bandwidth Reciprocity	81
4.3	The Ratio of Internal Variance to Total Variance	87
4.4	The Slope of the Fletcher Plot for Wide-Band Signals	88
4.4.1	Effective Signal Bandwidth	89
4.4.2	Energy Splatter	91
4.4.3	Enhancement of Spectral Contours	92
5.	APPENDICES	98
5.1	APPENDIX I -- Noise-Energy Distributions	98
5.1.1	The Gaussian Assumption	98
5.1.2	Effects of 'Realistic Filtering'	100
5.2	APPENDIX II -- Synthesis of Noise Waveforms	104
5.2.1	The Number of Components Required	104
5.2.2	Sampling Considerations	110
5.2.3	The Synthesis Algorithm	114

5.2.4	Preparation of DECtapes	118
5.2.5	On-Line Generation of Stimuli	118
5.2.6	Stimulus Sequencing	119
5.2.7	Level Calibration	123
5.2.8	Spectral Analysis	124
5.3	APPENDIX III -- Evaluation of Synthetic Noise	129
5.3.1	Amplitude Characteristics	129
5.3.2	The 'Energy' of Synthetic Noise Bursts	132
5.3.3	Discrimination of Intensity with Synthetic and Thermal Noises	134
5.4	APPENDIX IV -- Procedure for Fitting Lines to Fletcher Plots	139
6.	REFERENCES	141

List of Tables

1.1	Summary of band-widening experiments.	13
1.2	Cutoff frequencies for the final bandpass filter.	22
2.2	Masker bandwidths employed with each signal.	24
3.1	Results of parameter searches for listener JA.	31
3.2	Results of parameter searches for listener RB.	32
3.3	Parameter estimates based on pooled data.	37
3.4	Slope of reciprocity functions for various values of $W_n - W_s$.	56
4.1	Estimates of k.	69
A2.1	Number of components employed in the synthesis of noise bursts and the number of different bursts generated.	120
A2.2	Hum and distortion measurements of calibrating tone.	125
A3.1	Mean amplitudes of synthetic noises.	130
A3.2	Expected and observed number of zero-crossings and amplitudes exceeding 4 σ.	131
A3.3	Expected and observed mean 'energy' and relative variability of 'energy'.	133
A3.4	Thresholds obtained with synthetic and thermal noises.	137

List of Figures

1.1	Schematic Fletcher plot assuming a power-spectrum model.	4
1.2	Thresholds predicted by an energy-detection model.	9
2.1	Block diagram of apparatus.	18
3.1	Tonal threshold as a function of W_n and level.	26
3.2	Threshold of 50 Hz wide noise as a function of W_n and level.	28
3.3	Tonal threshold as a function of W_n.	33
3.4	Threshold of 50 Hz wide noise as a function of W_n.	35
3.5	Best-fitting Fletcher plots for tone and narrow-band noise.	38
3.6	Threshold of 500 Hz wide noise as a function of W_n and level.	41
3.7	Threshold of 792 Hz wide noise as a function of W_n and level.	43
3.8	Threshold of 500 Hz wide noise as a function of W_n.	45
3.9	Threshold of 792 Hz wide noise as a function of W_n.	47
3.10	Threshold as a function of W_s for conditions where $W_n = W_s$.	50
3.11	Threshold as a function of W_s for conditions where $W_n \geq W_c$.	52
3.12	Threshold as a function of W_s for various values of $W_n - W_s$.	54
3.13	Reciprocity factors as a function of $W_n - W_s$.	57
4.1	Schematic representation of internal signal processing.	63
4.2	Residual sum of squares as a function of k -- tonal signal.	70
4.3	Comparison of predicted and obtained tonal thresholds.	72
4.4	Residual sum of squares as a function of k -- 50 Hz signal.	77
4.5	Comparison of predicted and obtained narrow-band noise thresholds.	79

4.6	Predicted bandwidth reciprocity functions.	83
4.7	Bandwidth reciprocities as a function of $W_n - W_s$ for various values of k.	85
4.8	Pictorial representation of stimulus and internal spectrum.	94
A1.1	Threshold as a function of log df.	102
A2.1	Distribution of instantaneous amplitudes for a unit sinusoid.	105
A2.2	B_2 as a function of sample size.	108
A2.3	Pictorial representation of the effects of sampling on stimulus spectrum.	112
A2.4	Flow chart of the off-line synthesis routine.	116
A2.5	Flow chart of the on-line generation routine.	121
A2.6	Representative spectra.	126
A3.1	Block diagram of the apparatus for the experiment comparing intensity discrimination with thermal and synthetic noises.	135

1. INTRODUCTION

1.1 Detection of Tones Masked by Noise

1.1.1 The Power-Spectrum Model

In a classic paper on auditory masking, Fletcher (1940) showed that as the bandwidth of a masking noise is reduced from an initially large value, detection of a tonal signal centered in the masker band is virtually unaffected until some "critical bandwidth" is reached. Reducing the masker bandwidth below this critical value results in increased signal detectability. Fletcher argued that it is "as if" the listener were able to place an auditory bandpass filter in some stage of processing prior to the detector. Noise components remote from the signal frequency are, in effect, removed from the masker. As a first approximation, Fletcher assumed that this auditory filter was ideal -- having uniform gain within the passband and infinite attenuation outside the passband.

Fletcher studied the detectability of tones masked by noises of various bandwidths. Estimates of signal power (at threshold) were obtained as a function of masker bandwidth. The signal was always located at the center frequency of the masker. Three important results were obtained in this experiment: First, the ratio of signal power to noise spectral density required for detection of the tone in the presence of a 30 Hz wide noise band was found to be independent of signal frequency. This ratio was approximately 30. Second, signal threshold was found to increase with masker bandwidth until some value was exceeded. This "critical bandwidth" will hereafter be denoted as W_c. Fletcher interpreted the critical bandwidth as an estimate of the width of the auditory filter. Third, when the bandwidth of the masker was supra-critical, threshold was found to be an increasing function of signal frequency, in contrast to the result found with sub-critical bandwidth maskers.

The first two observations were interpreted as indicating that the process of detection includes a stage of filtering and that a signal would be just detectable when its

power equaled the power of the masker within the critical band. This equal-power hypothesis is the fundamental principle in Fletcher's model of detection. Estimates of critical bandwidth were obtained from plots of signal power at threshold as a function of masker bandwidth by drawing a line of unit slope through the threshold obtained with the 30 Hz masker and a line of zero slope through the threshold obtained with a wide-band masker. The value of bandwidth where these lines intersected was regarded as the critical bandwidth. The unit slope of the first line is a consequence of the equal-power hypothesis and the zero slope of the second line follows from the assumption of internal filtering. Critical bandwidths were shown to vary directly with signal frequency. This was consistent with the observed dependence of threshold on frequency with wide-band maskers.

Hawkins and Stevens (1950) measured tonal thresholds as a function of frequency using a wide-band noise as a masker. Armed with the equal-power hypothesis of Fletcher, these authors estimated critical bandwidths indirectly as the ratio of signal power to masker spectral density. Such indirect measurements of critical bandwidths have been termed "critical ratios" (Zwicker, Flottorp and Stevens, 1957) to distinguish them from estimates derived directly by varying masker bandwidth.

Critical ratios, when plotted as a function of frequency, parallel the critical bandwidth function reported by Fletcher but are only 40% as large. Scharf (1970) points out that, had Hawkins and Stevens assumed detection to require that signal power be only 40% of the effective masker power, then the two sets of measurements would be in close agreement. More recent studies of tones masked by sub-critical bandwidth noises (e.g., Hamilton, 1957; Swets et al., 1962; van der Brink, 1964; Greenwood, 1961; Weber, 1978; Sever and Small, 1979; Spiegel, 1979, 1981; Weir et. al., 1984) have also failed to confirm the equal power hypothesis of Fletcher. The equal-power assumption may be relaxed to require only that signal power be some fixed

proportion (P) of the effective masker power. Since detection is not independent of signal duration, we may express Fletcher's model in terms of signal energy:

$$\frac{E_s}{N_0} = P\ W_n; \qquad W_n < W_c,$$

$$\frac{E_s}{N_0} = P\ W_c; \qquad W_n \geq W_c. \tag{1.1}$$

The terms E_s, N_0, and W_n refer to the energy of the tonal signal, the spectral density of the masker, and its bandwidth, respectively.

It can be seen that this model predicts that a plot of signal energy (at threshold) as a function of masker bandwidth would consist of two line segments. A line of unit slope describes threshold variation with sub-critical values of W_n. A line of zero slope expresses the fact that threshold is independent of bandwidth for supra-critical maskers (see Figure 1.1). Plots of threshold as a function of masker bandwidth will be referred to as "Fletcher plots." The term "slope" will refer to the slope of the first line. Critical bandwidth is defined as the bandwidth at which the two lines intersect. We note that because of the difficulty in constructing narrow-bandwidth filters, Fletcher could not confirm the region of unit slope, although ample evidence for a second region of zero slope was presented.

We shall soon see that the predicted slope is determined by the mechanism of detection that is assumed and that the critical bandwidth represents an estimate of the bandwidth of the detection process. Since our main goal is to investigate the detection process, we are most interested in estimates of slope. The results predicted by an energy-detection model are considered next.

Figure 1.1

Schematic Fletcher plot assuming a power-spectrum model and a critical bandwidth of 300 Hz. At threshold, signal power is equal to the power of the masker within the critical band.

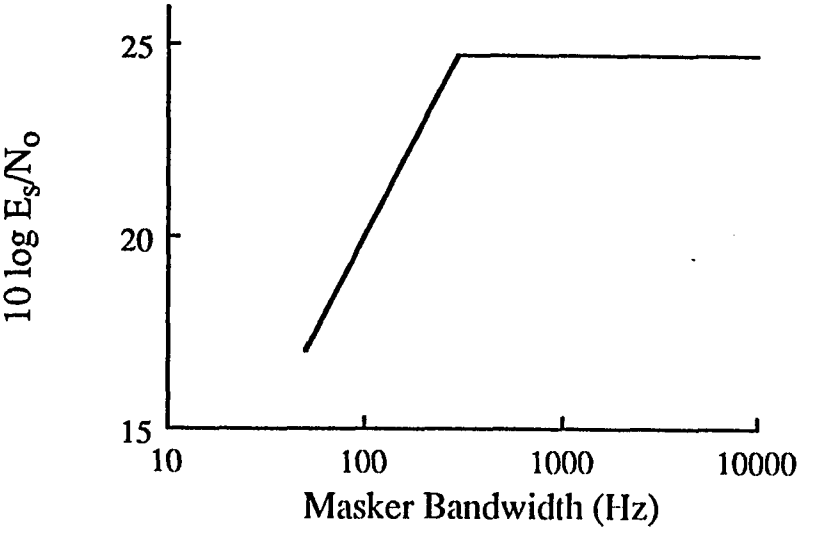
25
20
15
10 log E_s/N_o
10
100
1000
10000
Masker Bandwidth (Hz)

1.1.2 The Energy-Detection Model

A noise waveform represents the outcome of a stochastic process, hence more recent investigators have proposed models of detection which include limits imposed by stimulus variability. If detection is based on stimulus power, then it is appropriate to consider the statistics of power occurring during the observation intervals i.e., stimulus energy. The relevant properties of an energy-detection model are outlined below. A complete treatment may be found in Green and Swets (1974, chapter 8).

In a Two-Interval Forced-Choice (2IFC) task, an energy detector would examine the energy content of each observation interval and designate the one with the greatest value as the one which contained the signal. Since the energy content of a burst of noise is a random variable, it follows that an energy detector will vote incorrectly on some proportion of trials -- trials when the interval containing the signal is less energetic than the interval with only the masker. It is instructive to derive the distribution of energy conditional upon presentation of noise alone and also upon presentation of signal plus noise. Expressions relating the detectability of the signal to simple parameters of the masker can then be obtained.

Briefly, if the noise masker is represented with a Fourier series expansion, then the waveform is approximated as a sequence of $2W_nT$ points (in either the time or the frequency domain). The symbol T refers to the duration of the observation interval. Each of the $2W_nT$ points is an independent deviate from a Gaussian distribution with zero mean and variance proportional to the square of spectral density. A test statistic proportional to the power of the noise burst is obtained by summing the squares of all deviates. If the noise waveform is scaled to have unit spectral density then the test statistic is a random variable with a χ^2 density ($df = 2W_nT$; see Green and Swets, 1974, chapter 8). Since the mean of a χ^2 distribution is equal to the number of degrees

of freedom and the variance is given by 2df, the energy of a noise of finite duration may be modeled as a quantity equal to the product of the masker's spectral density (N_0) and a χ^2 deviate. It may be noted that an energy detector can be implemented by passing the stimulus waveform through a square-law device, and integrating the output of the device over the duration of the observation interval. A test statistic formed in this manner would be distributed as described above.

Processing the interval containing the tonal signal results in an energy variable which has the density of a non-central χ^2 and has $2W_nT$ df and non-centrality parameter λ. The mean of such a random variable is equal to the sum of df plus λ; the variance is given by twice the number of df plus four times λ.

In order to predict the performance of the detector, the probability that the energy of the signal interval exceeds that of the interval with noise alone must be determined. Since the detector bases its decisions solely on the values of the test statistics, the probability of a correct decision is equal to the probability that the energy of the signal interval exceeded that of the noise alone interval. Green and McGill (1970) have shown that the percent correct obtained with a tonal signal in a 2IFC task is given by the area beyond F = 1 of a non-central F distribution. The distribution has $2W_nT$, $2W_nT$ degrees of freedom and non-centrality parameter $2E_s/N_0$.

A more convenient expression for the detectability of the signal may be obtained by noting that when the number of degrees of freedom is large the densities associated with both intervals are approximately Gaussian. When this is so, the density of the difference distribution may also be considered to be Gaussian. Following Green and Swets (1974) we denote Ω as the listener's test statistic. The subscripts n or sn refer to the observation interval containing masker alone, or to the one containing the signal, respectively. The normalized mean $(\overline{\Omega}_{sn} - \overline{\Omega}_n)$ of the distribution of differences is

given by

$$\overline{\Omega}_{sn} - \overline{\Omega}_{n} = \frac{E_s/N_0}{\sqrt{2W_nT+2E_s/N_0}} \tag{1.2}$$

which is Eq. (8.13) in Green and Swets (1974).

The effect of masker bandwidth on detectability of a tonal signal can be observed by fixing the value of the mean of the difference distribution and determine how E_s/N_0 changes with W_n. Setting the mean to $1/\sqrt{2}$ yields approximately 76% correct responses. The quadratic may be solved for E_s/N_0 which yields,

$$\frac{E_s}{N_0} = \frac{1+\sqrt{1+4W_nT}}{2}. \tag{1.3}$$

Figure 1.2 is a plot of that function with an assumed duration of 0.1 sec. It is easily seen that on log-log coordinates, the function approximates a line with slope of ½ if the value of $2W_nT$ dominates the variance. When this is not true, threshold changes less rapidly with W_n. An energy detector's thresholds will vary with (at most) the square-root of masker bandwidth.

Spiegel (1979) has cautioned that since the normal approximation invoked for the density of the decision variable is known to become poorer with decreasing numbers of degrees of freedom, Eq. (1.2) may be in serious error for small bandwidth-duration products. These are precisely those conditions from which the slope of the Fletcher plot is estimated. Fortunately, it turns out that, with as few as 6 df, Eq. (1.2) accurately predicts required signal levels. This is demonstrated in APPENDIX I. Stated

Figure 1.2

Fletcher plot assuming an energy-detection model. Signal duration is equal to 100 msec.

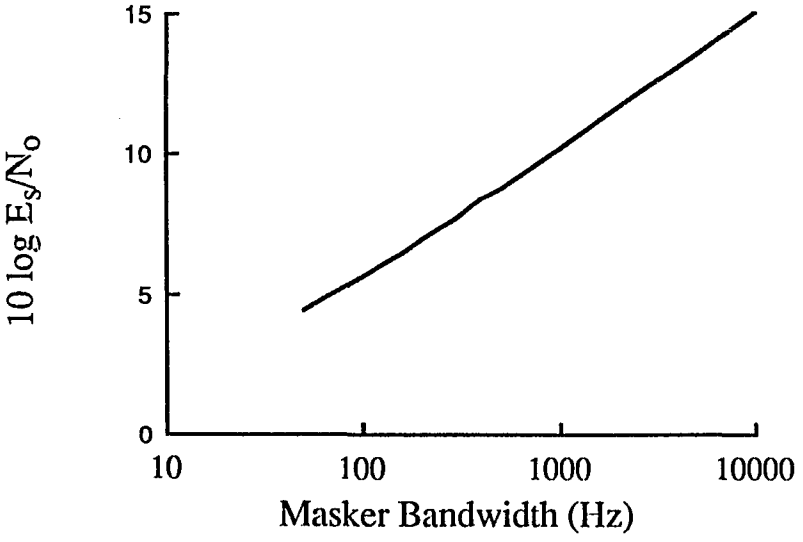
15
10
5
0
10 log E_s/N_o
10
100
1000
10000
Masker Bandwidth (Hz)

differently, the Gaussian assumption is tenable for the conditions under consideration.

Inspection of Figure 1.2 reveals that threshold is an ever-increasing function of W_n. If we assume an ideal bandpass filter Eq. (1.3) becomes

$$\frac{E_s}{N_0} = \frac{1+\sqrt{1+4W_nT}}{2}; \qquad W_n < W_c,$$
$$\frac{E_s}{N_0} = \frac{1+\sqrt{1+4W_cT}}{2}; \qquad W_n \geq W_c. \tag{1.4}$$

1.1.3 The Effect of Internal Filtering on Fletcher Plots

The first replication of Fletcher's study was performed by Schafer et. al. (1950). Noting that Fletcher used only a very few noises of sub-critical bandwidth, these investigators synthesized rectangular noise-bands to determine the form of the Fletcher plot. The synthetic noises were judged to be sufficiently similar to thermal noise as to be useful and had the advantage of having very sharp band edges.

The function relating threshold to masker bandwidth was found to be similar to that reported by Fletcher. However, these authors failed to find a sharp breakpoint at the critical bandwidth. Rather, the slope of the Fletcher plot changed gradually from unity to zero. The authors suggested that a tuned circuit might provide a better model of the critical bandwidth filter than the ideal filter originally suggested. The noise power at the output of a suitably chosen L-C-R circuit varies with the input bandwidth in the same manner as threshold varied with masker bandwidth.

Pfafflin and Mathews (1962) described the performance of an energy detector whose input was bandlimited by a Gaussian filter. In a later paper Mathews and Pfafflin (1965) showed that when the mean-square output of the Gaussian filter is matched to

that of a rectangular (i.e., ideal) filter, performance differs by 3 dB. The performance of an energy detector receiving a wide-band masker depends on the characteristics of the input filter. More recently, Patterson and Henning (1977) extended this observation and showed that the function relating E_s/N_0 to W_n was dependent on the shape of the input filter (see their Eq. 13). In particular they showed that with empirically derived filter shapes (see Patterson, 1976), the slope of the Fletcher plot is everywhere slightly less steep than one obtains with an ideal filter. Slope declines with increasing masker bandwidth reaching an asymptotic value of 0.5 dB per decade of W_n (see their Fig. 5). In APPENDIX I these findings are extended to a Gaussian filter.

Thus, if detection is based on either stimulus power or energy, replacing the ideal bandpass filter by a "realistic" filter results in a (slight) reduction of the slope. Furthermore, the transition from sub- to supra-critical bandwidth is not abrupt. The results of a band-widening experiment are relatively insensitive to the exact shape of the internal filter. This is consistent with the arguments of Patterson and Henning (1977). Precisely because of its insensitivity to the shape of the auditory filter, the band-widening experiment is well suited for examining the detection mechanism.

To summarize, the slope of the Fletcher plot depends on the details of the detection process. Fletcher's early power-spectrum model predicted unit slope on log-log coordinates. The more recent and more sophisticated energy detection model predicts that the slope is at most ½. The effect of substituting a "realistic" internal filter for the ideal band-pass is a slight reduction in the slope. Table 1.1 presents a review of band-widening experiments. It can be seen that most empirical estimates are steeper than predicted by the more sophisticated energy detection model.

Table 1.1

Estimates of the slope of the Fletcher plot from band-widening experiments. Signals were tones. The slope and method of determining slope are indicated.

Study	Slope	Method of Determination
Fletcher (1940)	1.0	Theory
Schaeffer et. al. (1950)	1.0	Theory
Hamilton (1957)	0.5	Empirical [a]
Greenwood (1961)	1.0	Theory
van der Brink (1964)	$.5 \leq slope \leq 1.0$	Empirical
Bos and de Boer (1966)	1.0	Empirical [a]
Weber (1978)	0.9	Empirical [b]
Sever and Small (1979)	0.8	Empirical [b]
Spiegel (1979)	0.7	Empirical [b]
Spiegel (1981)	2.3	Empirical [b]
Weir et. al. (1984)	0.5	Theory

(a) Data partition and lines of best-fit determined visually.
(b) Data partition and lines of best-fit determined by computation.

1.2 Detection of Noise Signals Masked by Noise

1.2.1 Power-Spectrum Model

It may be recalled that for the power-spectrum model, a signal is detectable when its power is some fixed proportion of the masker's power within the critical band. It follows that threshold does not depend on the spectral distribution of the signal within the critical band. The Fletcher plot should be described by

$$\begin{aligned} \frac{S_0}{N_0} &= P\,\frac{W_n}{W_s}; && W_n < W_c, \\ \frac{S_0}{N_0} &= P\,\frac{W_c}{W_s}; && W_n \geq W_c. \end{aligned} \tag{1.5}$$

The terms S_0 and W_s are the spectral density (at threshold) and the bandwidth of the noise signal. The proportionality constant is the same as with tonal signals. Indeed, $S_0 W_s$ should be equal to the power of the tone at threshold. The Fletcher plot obtained with a narrow-band noise signal should be the same as that obtained with a tone. Implicit in this is the independence of signal and masker waveforms.

1.2.2 Energy-Detection Model

Consider now the performance of an energy detector with a noise waveform as the signal. It is assumed that $W_s \leq W_n$. Schacknow and Raab (1976) showed that the normalized mean of the difference distribution

$$\overline{\Omega}_{sn} - \overline{\Omega}_n = \left[\frac{W_s T}{2}\right]^{1/2} \cdot \frac{S_0}{N_0} \cdot \frac{1}{\sqrt{W_n/W_s + S_0/N_0 + \tfrac{1}{2}(S_0/N_0)^2}}. \tag{1.6}$$

To observe the change in performance with increased masker bandwidth, the mean of the difference distribution is set to $1/\sqrt{2}$; solving for S_0/N_0 yields

$$\frac{S_0}{N_0} = \frac{1+\sqrt{4W_nT-2W_n/W_s+1}}{2W_sT-1}. \tag{1.7}$$

If variance due to the signal is small, then

$$\frac{S_0}{N_0} \approx \frac{\sqrt{W_n}}{W_s\sqrt{T}}. \tag{1.8}$$

It can be seen that threshold will increase with approximately the square-root of masker bandwidth. If the contribution of the variance due to the signal is not negligible, then a shallower slope is expected. This is the same as was true with tonal signals.

1.2.2.1 Effect of Signal Bandwidth on the Fletcher Plot

Energy-detection models do not customarily distinguish between narrow- and wide-band signals. Little is known about the effects of signal bandwidth on the slope of the Fletcher plot. As described earlier, slopes ranging between ½ and 1 are typically obtained with tonal signals. Noise signals, in contrast, may yield steeper slopes (Schacknow and Raab, 1976).

1.2.2.2 Bandwidth Reciprocity

Threshold varies with signal bandwidth both in theory and in practice. The decrease (in dB) of S_0/N_0 resulting from a decade increase in bandwidth is defined as the signal bandwidth reciprocity. This reciprocity is known to depend on the relationship between signal and masker bandwidth. Matched spectra (i.e., when

W_n=W_s) yield a 2 dB reciprocity. On the other hand, when a broadband masker is used, a reciprocity of about 6 dB is obtained (see Schacknow and Raab, 1976 for a review and also Spiegel, 1979; 1981).

The predictions of an energy-detection model, with respect to reciprocity, depend on assumptions about internal filtering. If the listener can always adjust the bandlimits of his internal filter so that W_c/W_s is some constant (not necessarily one), then a reciprocity of 5 dB is predicted. On the other hand, if the effective masker bandwidth is fixed and large, the predicted reciprocity is 10 dB.

1.3 Summary

As detection models have become more sophisticated, the values predicted for Fletcher plot slopes have been reduced. Fletcher's power-spectrum model predicted unit slope. Substituting a more "realistic" auditory filter reduced the slope somewhat. Incorporating stimulus variability into the model results in a slope of ½ or even less.

The available data, summarized in Table 1.1, indicate that slope is greater than predicted by the more recent model. Moreover, slope may depend on signal spectrum an effect not predicted by any model. Finally, signal bandwidth reciprocity is known to depend on whether masker bandwidth equals or exceeds signal bandwidth. The details of this dependency have not been established. From these considerations, it seems worthwhile to study the detectability of sub- and supra-critical bandwidth signals masked by noises of various bandwidths. Since, predictions depend on bandwidth specifications, analysis is simplified if we employ noises with rectangular spectra.

2. METHODS

Four experiments were conducted in a study of the detection process. Two experiments investigated the effects of masker bandwidth and level with sub-critical bandwidth signals: a tone and a 50 Hz band of noise. Two additional experiments examined the effects of masker bandwidth and level with signals that were wider than the critical band. These were 500 and 792 Hz wide noises. The study was designed, in addition, to examine the signal bandwidth-intensity reciprocity as a function of masker bandwidth. In all experiments, difference thresholds were determined with a 2IFC staircase procedure designed to track the signal level necessary for 73.6 percent correct detections. In all presentations, both the signal and masker were gated simultaneously.

2.1 Subjects

Two male graduate students (JA and the author) served as subjects. Both were experienced listeners and had received considerable training before any data were collected. Both listeners had audiologically normal hearing in the ear used for the task.

2.2 Apparatus

A block diagram of the apparatus employed is presented in Figure 2.1. In most conditions, both the signal and masker waveforms were synthesized off-line on a DEC PDP-8e minicomputer and stored in digital form on magnetic tape.

Employing a representation of noise developed by Rice (1954), noise bursts with nearly rectangular spectra (on average) were digitally synthesized by adding uniformly spaced sinusoidal components, each of unit amplitude and random starting phase. For all synthetic stimuli, at least 50 components were added to ensure that the resultant distribution of instantaneous amplitudes would be sensibly Gaussian (see APPENDIX II section 1). Additionally, it was required that the number of components be at least

Figure 2.1

Block diagram of apparatus.

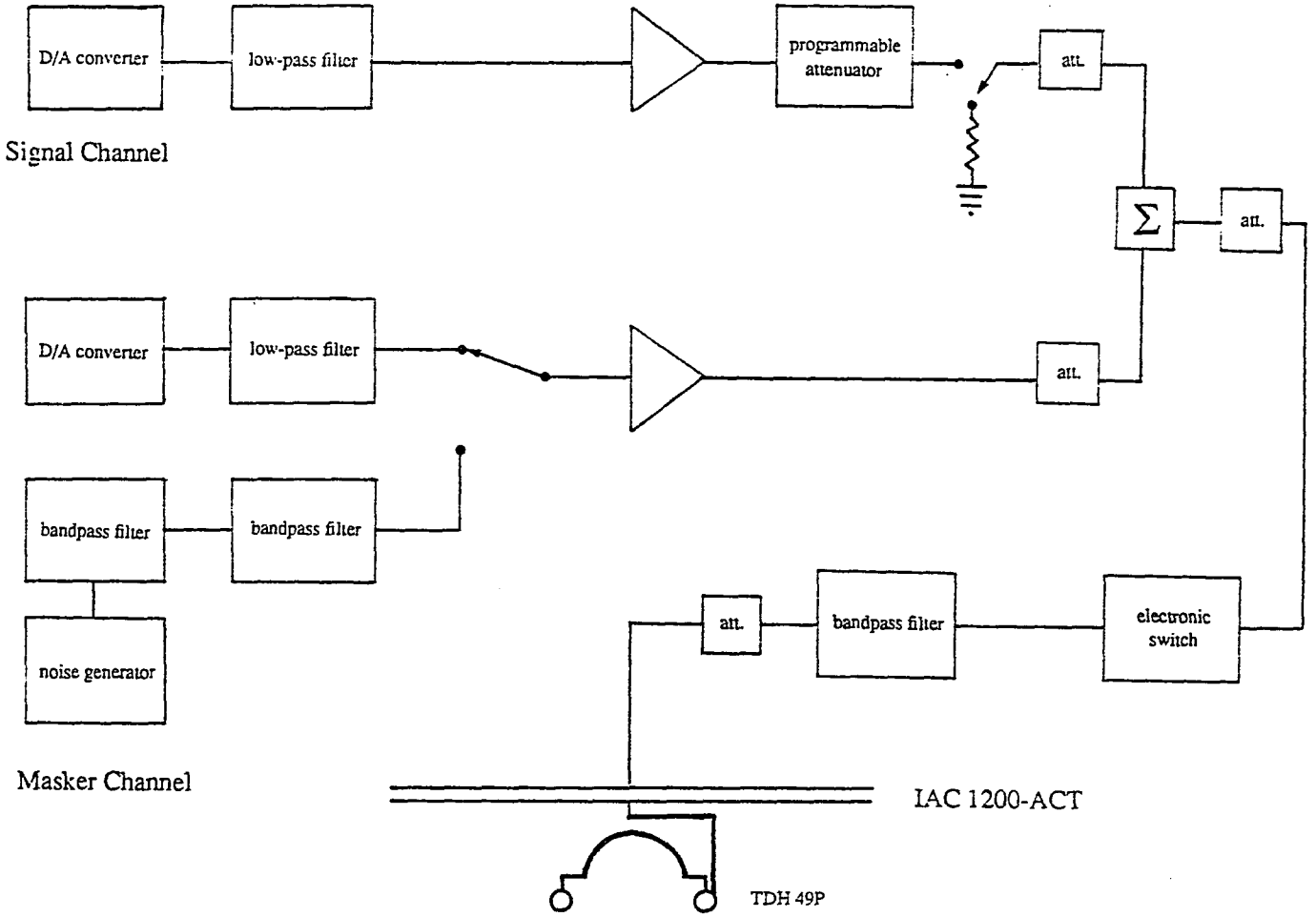
D/A converter
low-pass filter
programmable attenuator
att.
Signal Channel
Σ
att.
D/A converter
low-pass filter
att.
bandpass filter
bandpass filter
att.
bandpass filter
electronic switch
noise generator
Masker Channel
IAC 1200-ACT
TDH 49P

twice the product of bandwidth and duration (Green and Swets, 1974, section 6.3). Thus the distribution of energy across noise-bursts would approximate that of real noise stimuli having rectangular spectra. Results of the synthesis are compared with the Rice model of noise in APPENDIX III.

For each trial, two samples of signal and of masker were read from magnetic tape (DECtape) into the computer's memory and then transferred to digital-to-analog converters (D/A's) at the rate of 10,000 amplitudes per second. The outputs of the D/A's were led into separate low-pass anti-alias filters (Rockland 1042-F) having 48 dB per octave attenuation rates. The cutoff frequency was set to 1.4 times the highest frequency synthesized. This resulted for the "worst case" in 64 dB attenuation of the first alias component (see APPENDIX II section 2). All higher frequency components were further attenuated at the rate of 48 dB per octave. To obtain the widest bandwidth masker (5000 Hz), the output of a General Radio 1390-B noise generator was bandlimited by two Rockland 852 electronic filters connected in cascade. The resulting attenuation rate was 96 dB per octave.

The bandlimited waveforms (synthetic or thermal) were led to two channels -- one for the signal, the other for the masker. Each channel contained an amplifier (Calex 175) and attenuators for level adjustments. The magnitude of the signal was controlled by means of a Grason-Stadler 1284 programmable attenuator. The activation of a "signal" relay placed the signal in one of the two observation intervals with a probability of 0.5 -- determined by a Coulbourn S35-20 probability generator. At the beginning of each experimental session, the computer generated a 1000 Hz tone for calibration of levels (see APPENDIX II section 7).

In all conditions, the signal and masker waveforms were added by means of a resistive mixing network. For the synthetic waveforms, stimulus sequencing ensured

that the same signal-plus-masker waveform was not repeated during a threshold determination. Stimuli were gated by a Grason-Stadler electronic switch (1287-B) set to have 5 msec rise/fall times. The waveforms were then passed through a Rockland 852 bandpass filter. Cutoff frequencies were set to be 2/3 and 3/2 times the masker's lower and upper frequency components, respectively (see Table 2.1). The waveforms were then passed through a master attenuator, patched into a sound-proof chamber (IAC 1200-ACT), and finally delivered to the subject's earphone (TDH 49-P), mounted in a MX/41-AR cushion.

Stimulus sequencing, signal levels, and data acquisition were controlled on-line by a DEC PDP-8e computer. At the end of a threshold determination, the computer provided a frequency histogram of signal levels visited.

2.3 Procedures

2.3.1 Psychophysical Method

Difference thresholds were determined using a 2IFC adaptive procedure designed to minimize starting level bias (Moschetto, Bernstein and Raab, 1980). A faint warning click, presented to the subject's contralateral earphone, marked the beginning of each trial. Two 102.4 msec (including rise/fall times) observation intervals, whose onsets were spaced 800 msec apart, were presented in succession one second after the warning click. The signal was placed with equal probability in one of the two observation intervals. The subject indicated the interval containing the signal by pressing one of two microswitch buttons. Indicator lights on the response panel marked the observation intervals and provided immediate performance feedback. Trials were self-paced, which yielded one trial approximately every six seconds.

Each threshold determination began with the signal clearly audible. The following "hybrid" decision rule was employed: Two correct responses before an error resulted in

Table 2.1

Cutoff frequencies for the final bandpass filter.

Bandwidth (Hz)	Filter Settings	
	Lower	Upper
50	983	2288
63	979	2298
79	974	2310
100	967	2327
158	948	2372
500	847	2657
629	812	2771
792	770	2921
1000	721	3122
1256	665	3381
1581	443	3729
5000	277	8123

1.5 dB attenuation of the signal. After the first error (first reversal), five correct responses before two errors resulted in 1.5 dB attenuation of the signal. Otherwise the signal was increased by 1.5 dB. Each determination was terminated when the subject completed 70 trials after the first reversal. Only those levels visited after the first reversal were included in the determination of the threshold. Upon completion of a run, the median signal level revisited was computed and converted to E_s (for tonal signals) or S_0 (for noise signals). The ratio of E_s/N_0 or S_0/N_0, expressed in decibels, is used as an index of discrimination. Five such determinations were made for each experimental condition.

2.3.2 Experimental Design

Experiment 1 investigated the effects of masker bandwidth and level on the detection of a tonal signal. The tone was computer generated, always beginning at a positive-going zero-crossing. Signal duration was 102.4 msec. Masker bandwidths ranged from 50 to 5000 Hz (see Table 2.2), geometrically centered on the signal frequency -- 1500 Hz. Masker noise-power density (N_0) was either 8 or 38 dB SPL. Thus for the widest masker bandwidth employed, overall level was 45 or 75 dB SPL.

Experiments 2 - 4 were similar except that the signals to be detected were bands of noise (50, 500 and 792 Hz wide, respectively) geometrically centered at 1500 Hz (see Table 2.2). In all conditions, the masker bandwidth equaled or exceeded that of the signal. The order of presentation was blocked by type of signal and masker level, with the order of masker bandwidth randomized. Both signal type and masker level were scrambled across subjects.

Table 2.2

Masker bandwidths employed with the tone and noise signals.

Signal				Masker Bandwidth (Hz)
Tone	Noise			
	50 Hz	500 Hz	792 Hz	
X	X			50
X	X			63
X	X			79
X	X			100
X	X			158
X	X	X		500
X	X	X		629
X	X	X	X	792
X	X	X	X	1000
X	X	X	X	1256
X	X	X	X	1581
X	X	X	X	5000

3. RESULTS

3.1 Sub-Critical Bandwidth Signals

3.1.1 Detectability as a Function of Masker Bandwidth

One of the principal objectives of the present series of studies is to examine the change of signal threshold with increasing masker bandwidth (W_n). We begin by presenting each listener's data organized into plots of mean threshold as a function of masker bandwidth ("Fletcher plots"). Thresholds for the tone and 50 Hz noise are presented in Figures 3.1 and Figure 3.2, respectively. In all cases the parameter is the masker spectral density (N_0). Two general features of the plots are evident: Signal threshold initially increases with W_n and then becomes relatively independent of masker bandwidth. That is, as Fletcher (1940) suggested, only noise masker components "near" the signal contribute significantly to the masking of that signal. Stated otherwise, the listener's processing of stimuli includes a stage of spectral selectivity (internal filtering) prior to the decision stage.

Since we do not know *a priori* the extent of a listener's spectral selectivity, we must begin by partitioning the data into two sets: thresholds for maskers within the passband of the internal filter and those for maskers whose bandwidths exceed the internal filter width (critical bandwidth). With the data so partitioned, parameters of both line segments may be estimated. We estimate each critical bandwidth from the intersection of the two line segments (Scharf, 1970). To do these estimations, an iterative least-squares residual procedure (Bogartz, 1968) was employed separately for each listener, signal, and level (see APPENDIX IV for details). The results of these parameter searches are presented in Tables 3.1 and 3.2, and are plotted as the solid lines in Figures 3.1 and 3.2.

Figure 3.1

Tonal threshold as a function of masker bandwidth. Filled squares: N_0 = 8 dB. Open squares: N_0 = 38 dB. Solid lines are best-fitting pairs of lines. Dashed lines indicate adjusted values (see text for details). Top: data from listener JA. Bottom: data from listener RB.

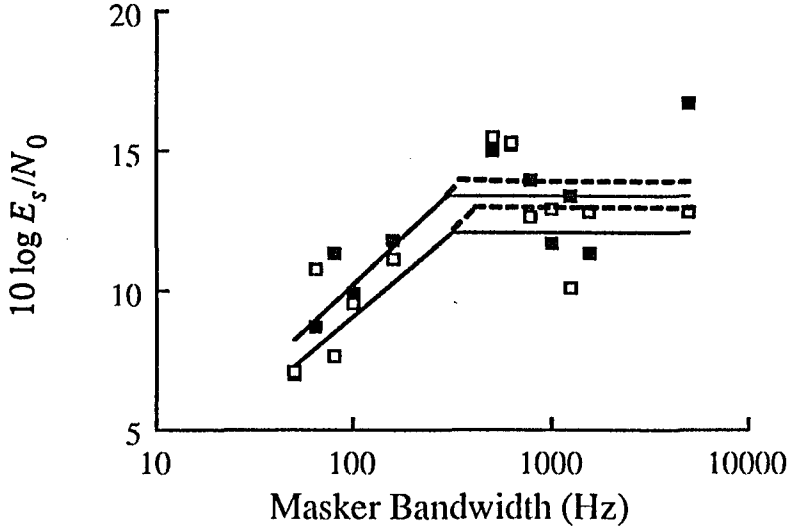
20
15
10
5
10 log E_s/N_0
10
100
1000
10000
Masker Bandwidth (Hz)

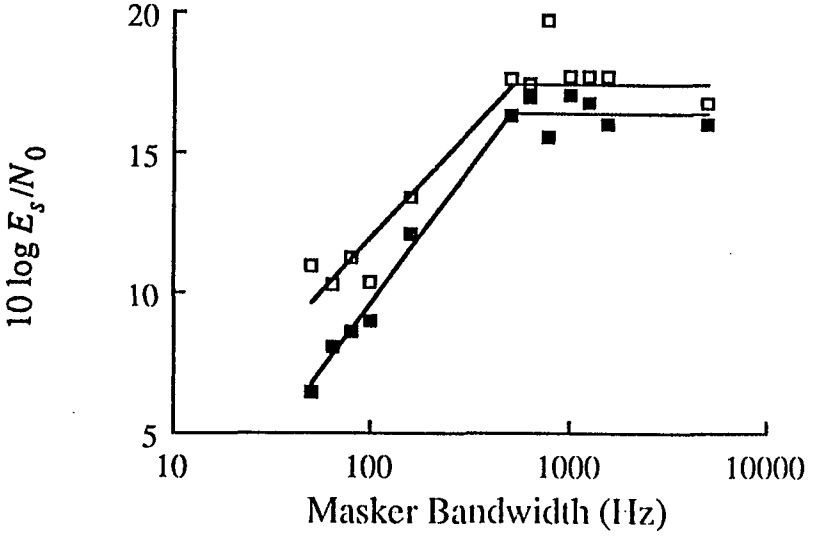
20
15
10
5
10 log E_s/N_0
10
100
1000
10000
Masker Bandwidth (Hz)

Figure 3.2

Threshold of 50 Hz wide noise as a function of masker bandwidth. Filled squares: N_0 = 8 dB. Open squares: N_0 = 38 dB. Solid lines are best-fitting pairs of lines. Dashed lines indicate adjusted values (see text for details). Top: data from listener JA. Bottom: data from listener RB.

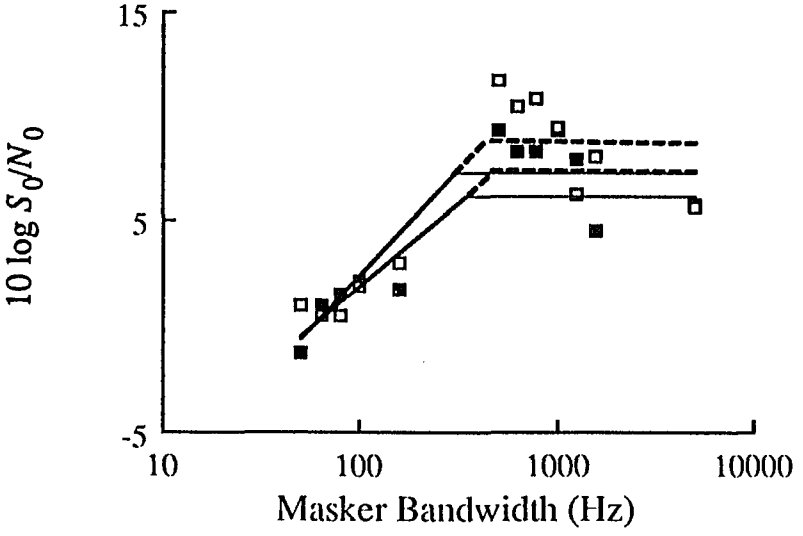
15
5
-5
10 log S_0/N_0
10
100
1000
10000
Masker Bandwidth (Hz)

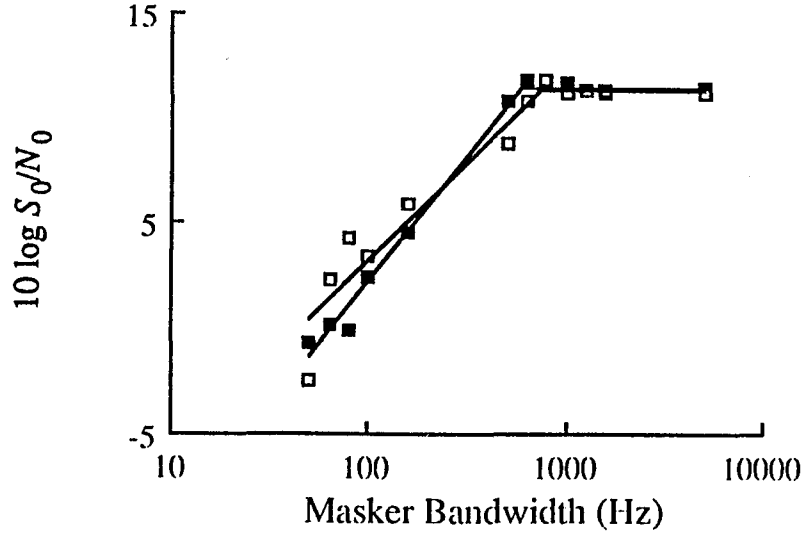
15
5
-5
10 log S_0/N_0
10
100
1000
10000
Masker Bandwidth (Hz)

Inspection of Figures 3.1 and 3.2 reveals that the estimates of each initial line segment well describe the subjects' performance. However, for subject JA, thresholds from maskers whose bandwidths are near W_c are somewhat poorer than those obtained with wider bandwidth maskers. The second line segments do not adequately describe performance. Since the estimates selected for the initial line segments correlated well with the data, we retain those line segments and adjust the intercepts of the second lines to obtain better fits. To do this, we used the original critical bandwidth estimate as the point of data partition, and calculated new intercepts. Again, we regard the intersection of the two lines as an estimate of critical bandwidth. The adjusted parameter estimates are presented as the dashed lines in Figures 3.1, 3.2, and in parenthesis in Tables 3.1 and 3.2.

3.1.2 Effect of Masker Level

Since studies of tones masked by noise and of noise masked by noise typically obtain Weber's law (e.g., Hawkins and Stevens, 1950; Miller, 1947) and since inspection of individual Weber fractions (presented in Figures 3.1 and 3.2) do not reveal systematic differences with level, we reanalyze our data sets, pooling observations from both masker levels. The new parameter estimates are presented in Table 3.3; mean thresholds are plotted as a function of masker bandwidth in Figures 3.3 and 3.4. For subject JA, adjusted values are also presented. These estimates from pooled data do not seem to differ from those obtained at either masker level.

3.1.3 Comparison of the Masking of the Tone and Narrow-Band Noise Signals

The noise signal employed in Experiment 2 was, as expected, narrower than the critical bandwidth estimates from the tonal signal. It is of interest, therefore, to compare performance with each type of signal. We note that for each subject, initial line segments for both signals have similar slopes. Furthermore, estimates of critical

Table 3.1

Results of parameter searches for listener JA.

Signal		Initial Line Segment		Critical Width [a]	
	N_0	Slope	Intercept		
Tone	8	0.67	-3.2	300	(354)
	38	0.60	-2.8	318	(435)
Noise-bands					
50 Hz	8	0.80	-14.0	345	(536)
	38	1.02	-17.9	304	(439)
500 Hz	8	2.18	-62.1	1034	
	38	3.36	-93.2	775	
792 Hz	8	3.24	-97.7	962	
	38	2.00	-61.8	986	

(a) adjusted values are in parenthesis. See text for details.

Table 3.2

Results of parameter searches for listener RB.

Signal	N_0	Initial Line Segment Slope	Intercept	Critical Width
Tone	8	0.96	-9.6	508
	38	0.78	-3.6	521
Noise-bands				
50 Hz	8	1.20	-21.7	589
	38	0.94	-15.6	710
500 Hz	8	1.95	-55.7	968
	38	2.26	-64.1	808
792 Hz	8	6.88	-204.4	964
	38	6.16	-182.8	1019

Figure 3.3

Tonal threshold as a function of masker bandwidth. Data were pooled across masker levels. Solid lines are the pair of best-fitting lines. The dashed lines indicate an adjusted value (see text). Top: data from listener JA. Bottom: data from listener RB.

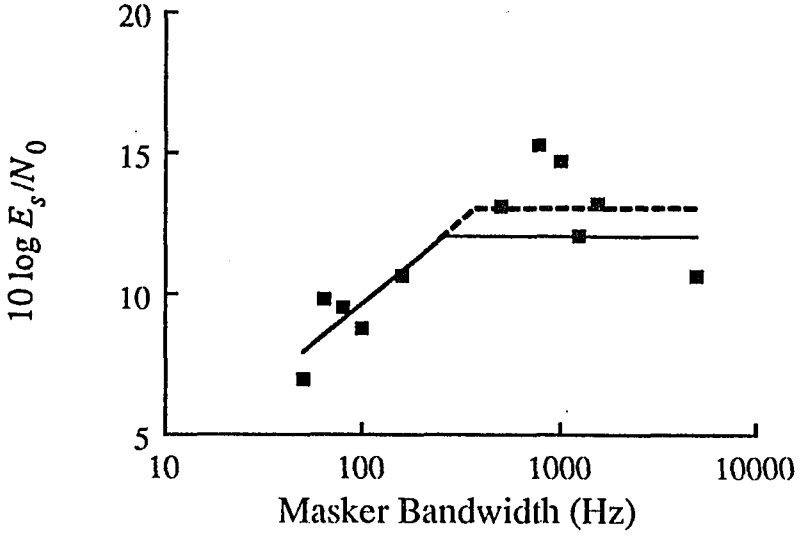
20
15
10
5
10 log E_s/N_0
10
100
1000
10000
Masker Bandwidth (Hz)

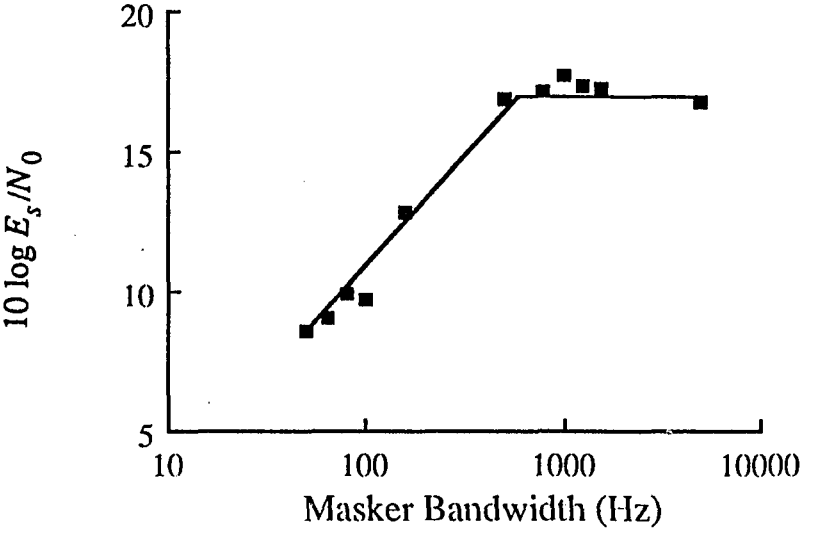
20
15
10
5
10 log E_s/N_0
10
100
1000
10000
Masker Bandwidth (Hz)

Figure 3.4

Threshold of 50 Hz wide noise as a function of masker bandwidth. Data were pooled across masker levels. Solid lines are the pair of best-fitting lines. Dashed lines indicate an adjusted value (see text for details). Top: data from listener JA. Bottom: data from listener RB.

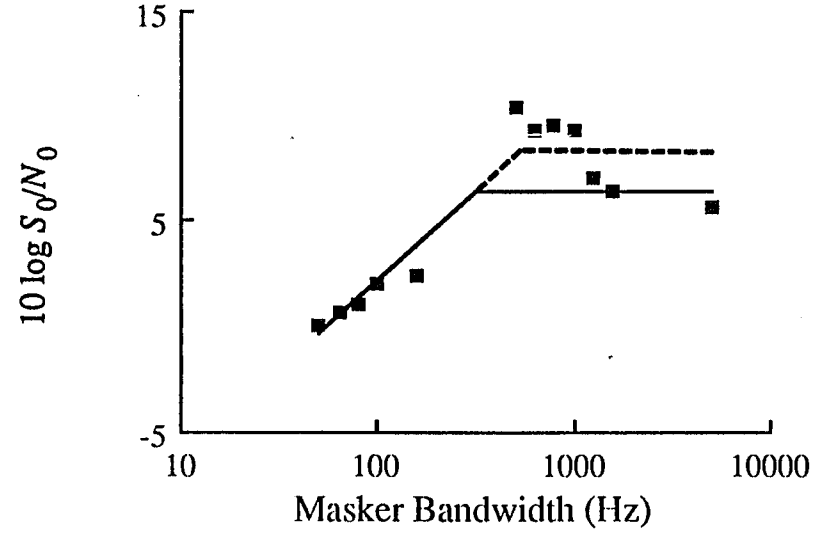
15
5
-5
10 log S_0/N_0
10
100
1000
10000
Masker Bandwidth (Hz)

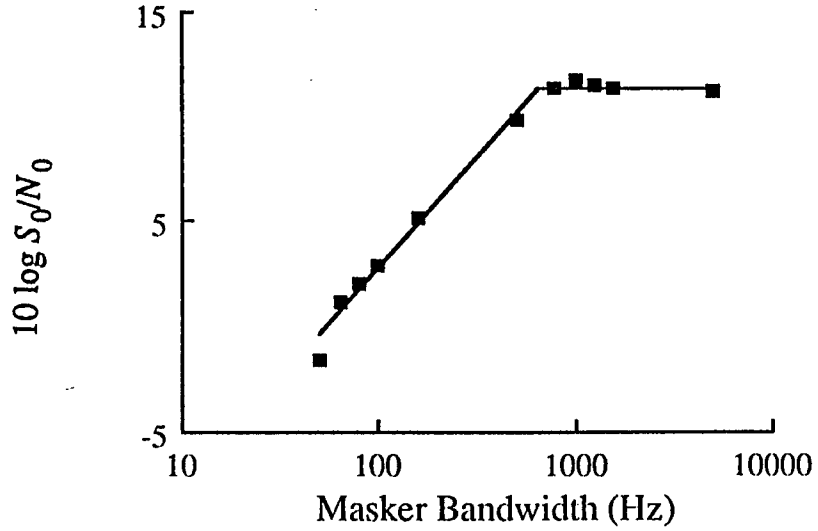
15
5
-5
10 log S_0/N_0
10
100
1000
10000
Masker Bandwidth (Hz)

Table 3.3

Parameter estimates for listeners JA and RB. Data were pooled across levels.

Signal	Listener	Initial Line Segment Slope	Intercept	Critical Width [a]	
	JA	0.59	-2.1	258	(379)
Tone	RB	0.81	-5.6	588	
	Mean	0.71	-3.8	423	(488)
Noise-bands					
	JA	0.86	-15.0	314	(522)
50 Hz	RB	1.06	-18.4	659	
	Mean	0.96	-16.7	487	(592)
	JA	2.77	-77.8	868	
500 Hz	RB	2.51	-71.3	974	
	Mean	2.64	-74.6	921	
	JA	2.62	-79.7	971	
792 Hz	RB	6.52	-193.6	990	
	Mean	4.57	-136.7	980	

(a) adjusted values are in parenthesis. See text for details.

Figure 3.5

Best-fitting Fletcher plots for tone and narrow-band noise. Top: based on data from listener JA. Bottom: based on data from listener RB.

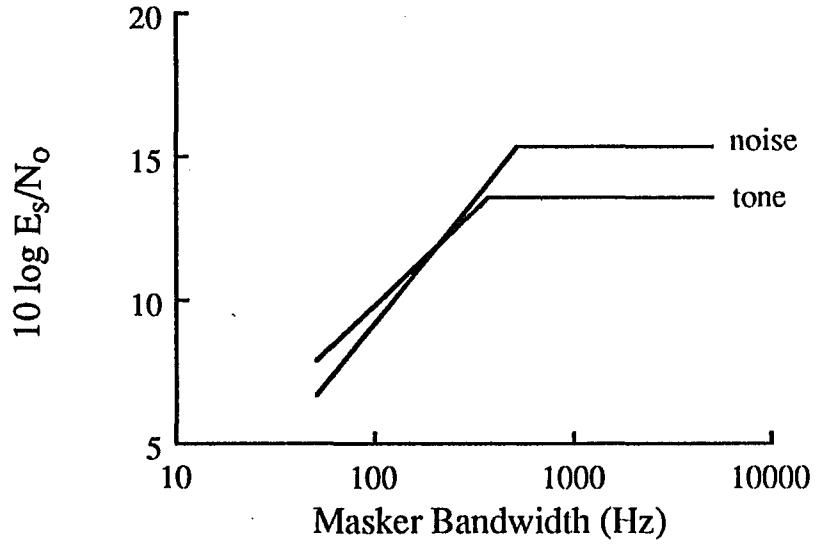
20
15
10
5
10 log E_s/N_o
noise
tone
10
100
1000
10000
Masker Bandwidth (Hz)

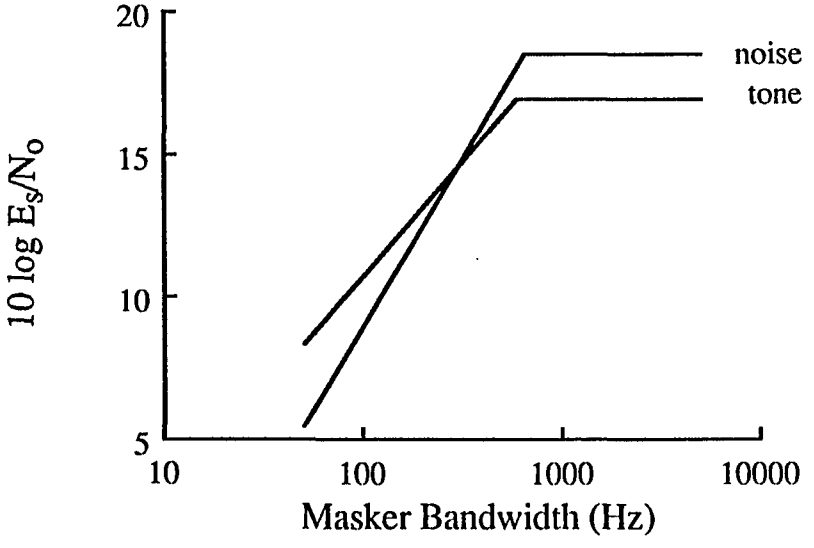
20
15
10
5
10 log E_s/N_o
noise
tone
10
100
1000
10000
Masker Bandwidth (Hz)

bandwidths from both signals are similar. The Fletcher plots are therefore parallel. We may directly compare signal thresholds by computing the ratio of signal energy-to-masker spectral density (E_s/N_0) required for detection for both types of signals. These best fitting Fletcher plots are presented in Figure 3.5. No systematic differences are evident; tones and narrow-band noises are masked similarly.

3.2 Supra-Critical Bandwidth Signals

3.2.1 Effect of Masker Bandwidth

Mean thresholds for the supra-critical bandwidth signals (W_s = 500 Hz and 792 Hz) were organized into Fletcher plots. Figures 3.6 and 3.7 present the thresholds of the 500 Hz and 792 Hz wide noises, respectively. In all plots, the parameter is the spectral density (N_0) of the masker. As was true with the narrow-band signals employed in Experiments 1 and 2, signal threshold increases with masker bandwidth until some critical width is reached. Increases beyond this critical width do not seem to elevate signal thresholds. It appears that, detection of these wide-band signals also includes a stage of internal filtering. As was the case with narrow-band signals, performance can be described by two line segments. Estimates of the parameters for these lines were obtained with the same procedure as that described earlier. These estimates are presented in Tables 3.1 and 3.2; the lines are plotted in Figures 3.6 and 3.7.

3.2.2 Effect of Masker Level

The data (presented in Figures 3.6 and 3.7) do not exhibit systematic departures from Weber's law. To obtain more reliable parameter estimates, we reanalyze the parameter space, employing all threshold determinations for a given subject and signal. These estimates are presented in Table 3.3 and in Figures 3.8 and 3.9, and do not differ from the estimates at either level.

Figure 3.6

Threshold of 500 Hz wide noise as a function of masker bandwidth. Filled squares: N_0 = 8 dB. Open squares: N_0 = 38 dB. Solid lines are best-fitting pairs of lines. Top: data from listener JA. Bottom: data from listener RB.

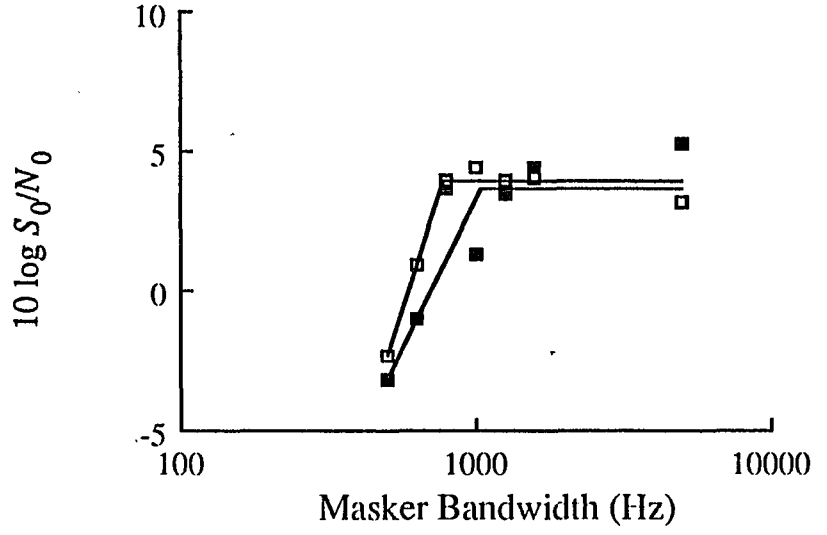
10
5
0
-5
10 log S_0/N_0
100
1000
10000
Masker Bandwidth (Hz)

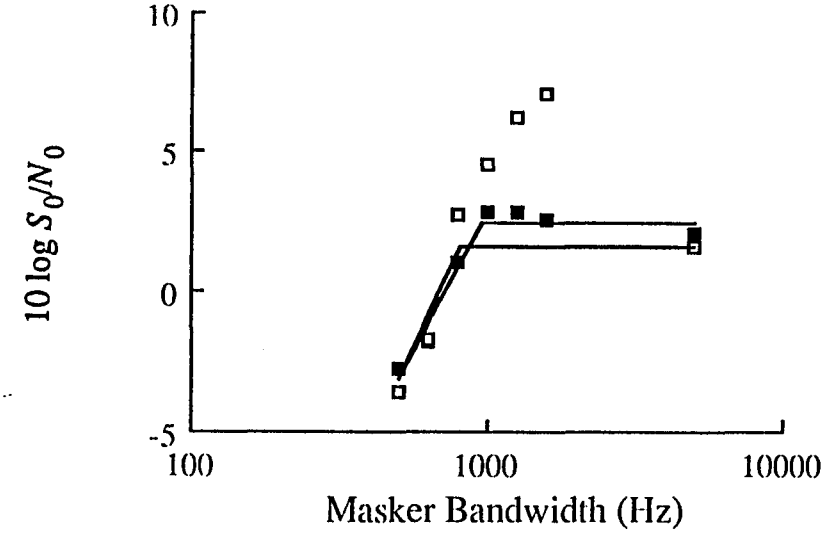
10
5
0
-5
10 log S_0/N_0
100
1000
10000
Masker Bandwidth (Hz)

Figure 3.7

Threshold of 792 Hz wide noise as a function of masker bandwidth. Filled squares: N_0 = 8 dB. Open squares: N_0 = 38 dB. Solid lines are best-fitting pairs of lines. Top: data from listener JA. Bottom: data from listener RB.

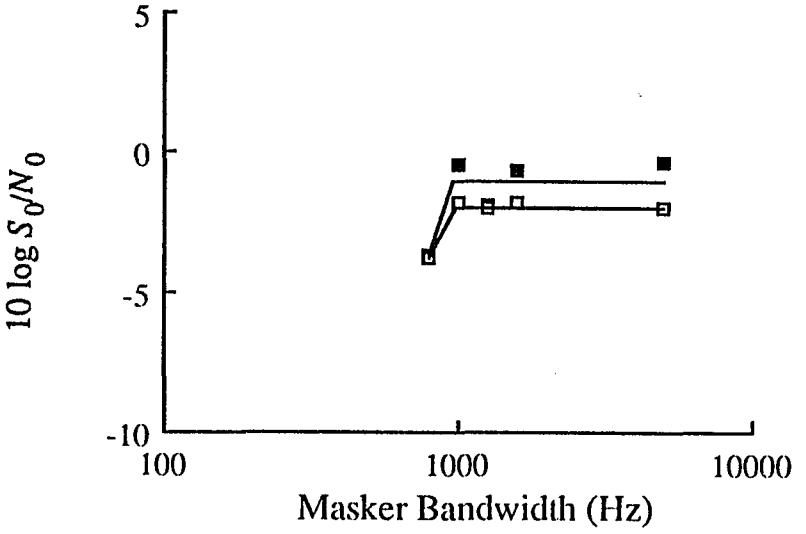
5
0
-5
-10
10 log S_0/N_0
100
1000
10000
Masker Bandwidth (Hz)

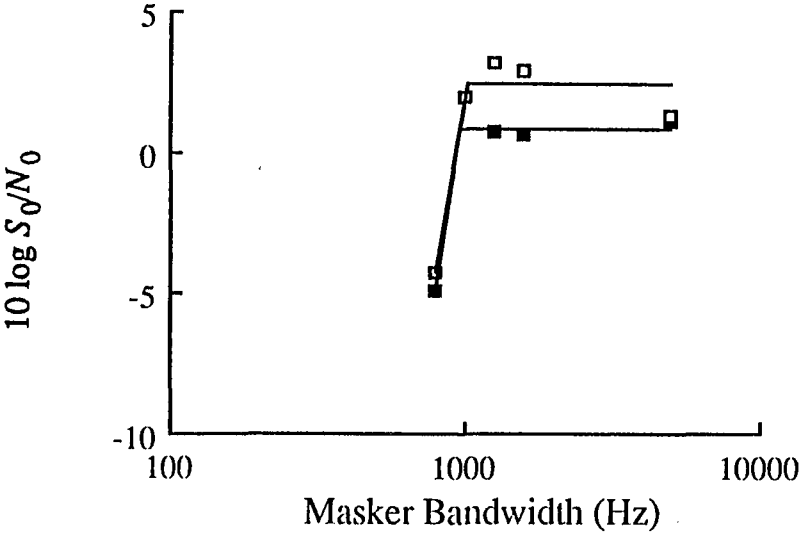
5
0
-5
-10
10 log S_0/N_0
100
1000
10000
Masker Bandwidth (Hz)

Figure 3.8

Threshold of 500 Hz noise as a function of masker bandwidth. Data were pooled across levels. Solid lines are the pair of best-fitting lines. Top: data from listener JA. Bottom: data from listener RB.

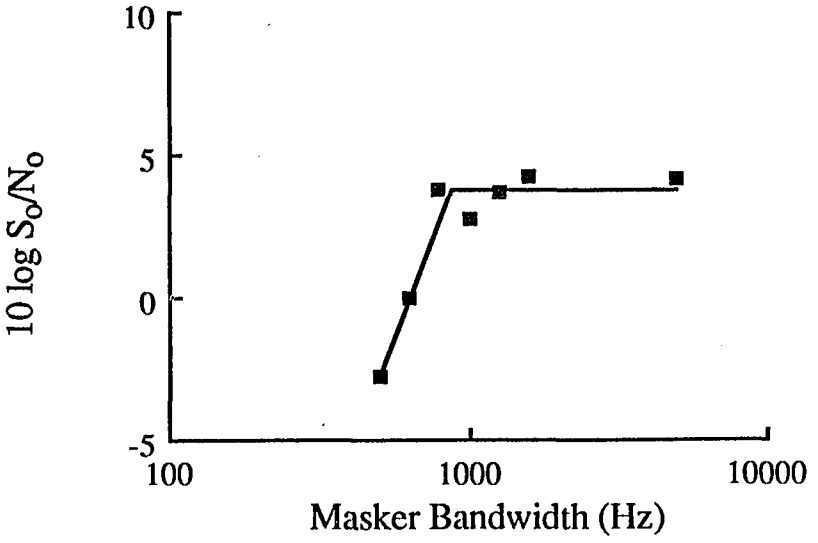
10
5
0
-5
10 log S_o/N_o
100
1000
10000
Masker Bandwidth (Hz)

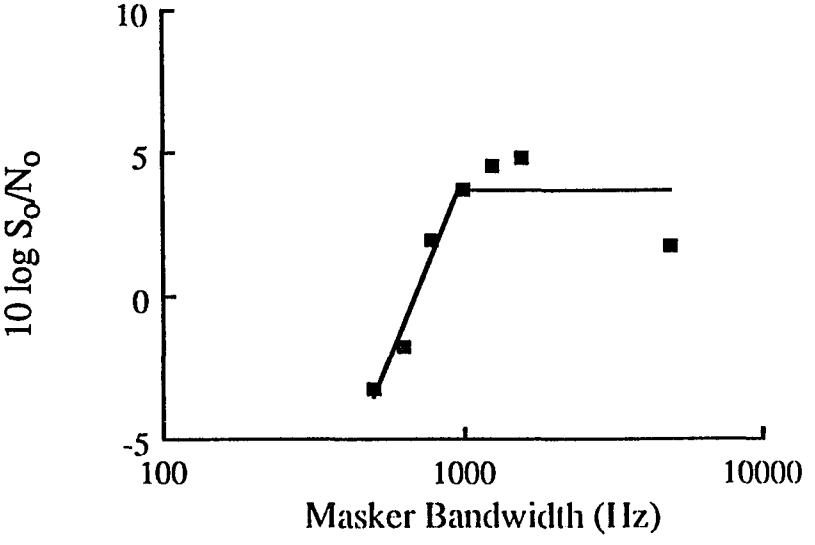
10
5
0
-5
10 log S_o/N_o
100
1000
10000
Masker Bandwidth (Hz)

Figure 3.9

Threshold of 792 Hz noise as a function of masker bandwidth. Data were pooled across levels. Solid lines are the pair of best-fitting lines. Top: data from listener JA. Bottom: data from listener RB.

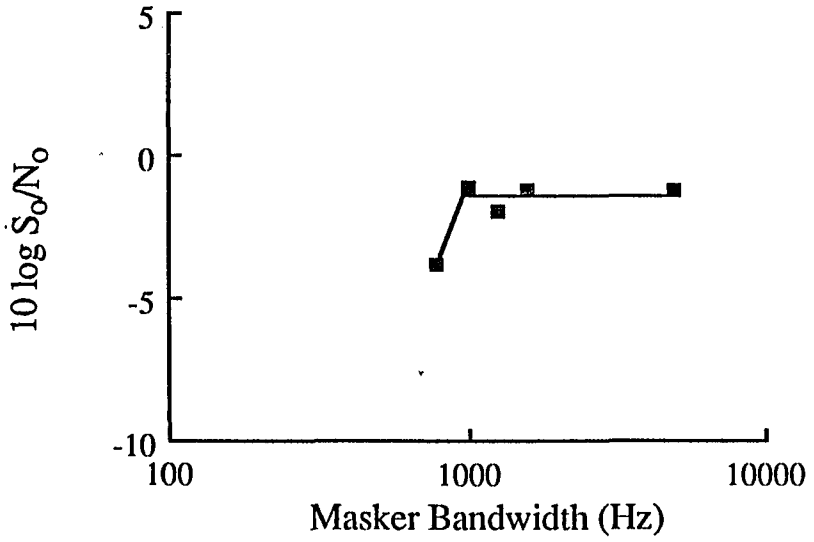
5
0
-5
-10
10 log S_o/N_o
100
1000
10000
Masker Bandwidth (Hz)

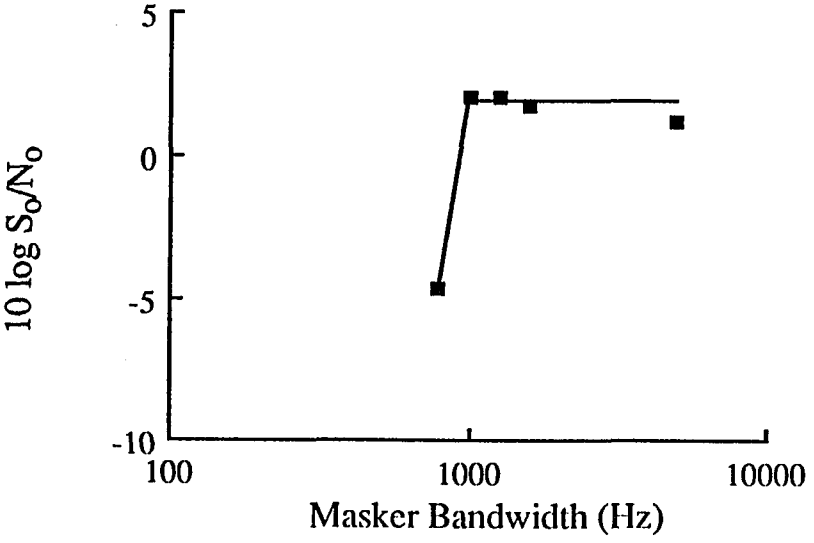
5
0
-5
-10
10 log S_o/N_o
100
1000
10000
Masker Bandwidth (Hz)

3.2.3 Effect of Signal Bandwidth

3.2.3.1 Critical Width

Inspection of Table 3.3 reveals that estimates of W_c derived from "sub-critical" signals (experiments 1 and 2) are smaller than those derived from "supra-critical" signals (experiments 3 and 4). Furthermore, the magnitude of W_c is an orderly function of signal bandwidth. It appears that listeners adjust the bandwidth of the detection process in accord with spectrum of the signal.

3.2.3.2 Bandwidth Reciprocity

When signal and masker waveforms have the same bandlimits, increases in bandwidth result in improved performance. Plotted in Figure 3.10 are mean thresholds (in dB) as a function of log bandwidth for these conditions. The slopes of the best-fitting lines (least-squares criterion) are -2.5 and -3.2 for listeners JA and RB respectively. When signal and masker have identical spectra, a ten-fold increase in bandwidth, yields approximately 3 dB of improvement in performance. These reciprocities are consistent with those previously reported (Small et al., 1959; de Boer, 1965; Bos and de Boer, 1966; Raab and Goldberg, 1975; Moore and Raab, 1975; Moore, 1975; Schacknow and Raab, 1976).

Performance also improves with increasing signal bandwidth when the maskers are supra-critical. Figure 3.11 presents signal-to-noise ratios for masker bandwidths that were in each case supra-critical. The slopes of the best-fitting lines are -5.7 and -8.5 for JA and RB, respectively. These reciprocities are consistent with those reported from studies employing fixed, wide-band maskers (Green, 1960; Campbell, 1964; Schacknow and Raab, 1976; Spiegel, 1979; 1981). Performance improves nearly 7 dB with a ten-fold increase in signal bandwidth. Clearly, the rate of improvement depends

Figure 3.10

Threshold as a function of signal bandwidth for conditions where signal bandwidth equaled masker bandwidth. Thresholds were averaged across levels. Solid line are the best-fits. Top: data from listener JA. Bottom: data from listener RB.

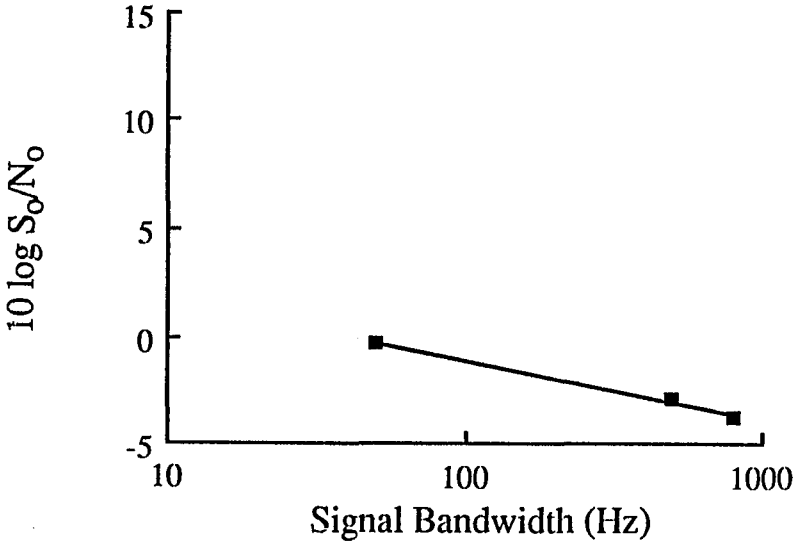
15
10
5
0
-5
10 log S_o/N_o
10
100
1000
Signal Bandwidth (Hz)

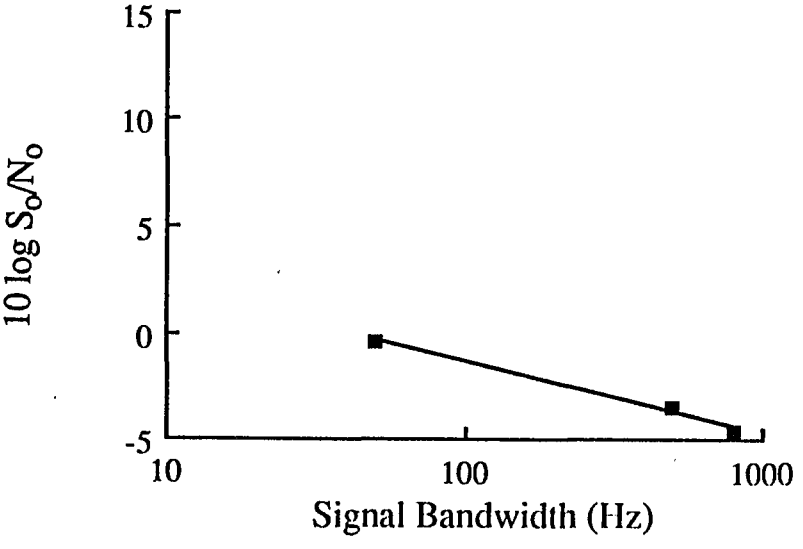
15
10
5
0
-5
10 log S_o/N_o
10
100
1000
Signal Bandwidth (Hz)

Figure 3.11

Threshold as as function of signal bandwidth for conditions where masker bandwidth exceeded each signal's 'critical' bandwidth. Thresholds were averaged across masker levels. Solid line are the best-fits. Top: data from listener JA. Bottom: data from listener RB.

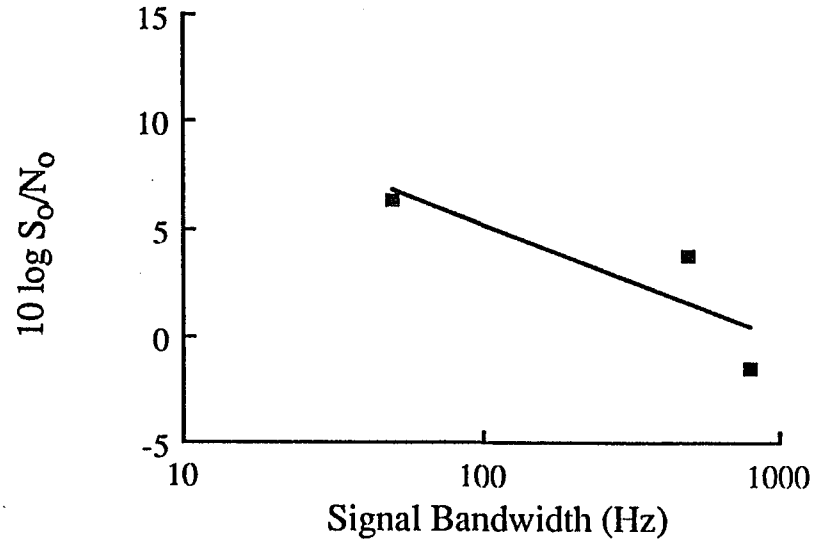
15
10
5
0
-5
10 log S_o/N_o
10
100
1000
Signal Bandwidth (Hz)

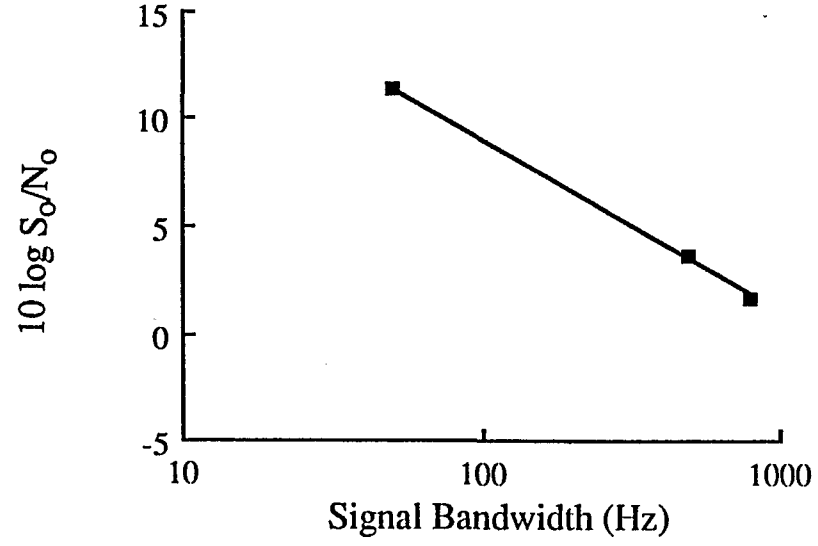
15
10
5
0
-5
10 log S_o/N_o
10
100
1000
Signal Bandwidth (Hz)

Figure 3.12

Threshold as a function of signal bandwidth for various values of the difference between masker and signal bandwidths (W_n–W_s). Thresholds not sampled were interpolated from appropriate Fletcher plots (see text). The solid lines are best-fits. Top: data from listener JA. Bottom: data from listener RB.

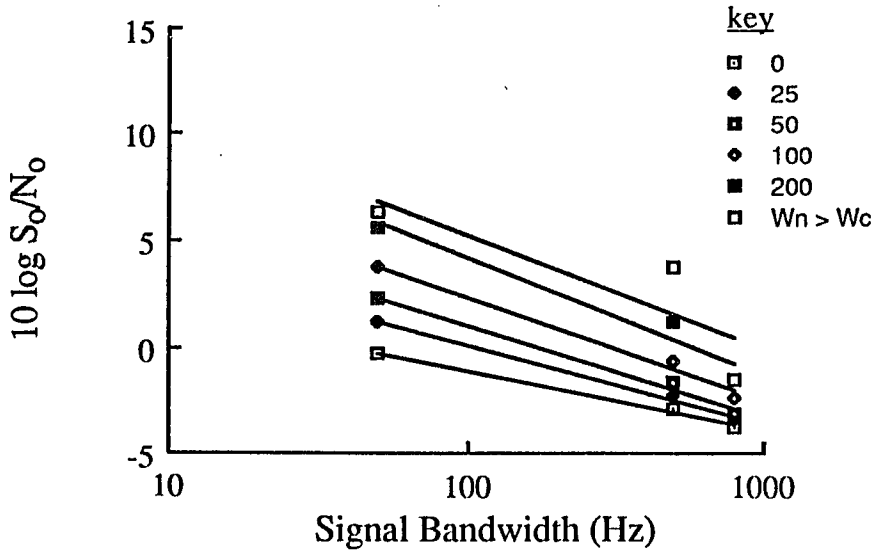
key
0
25
50
100
200
Wn > Wc
15
10
5
0
-5
10
100
1000
10 log S_o/N_o
Signal Bandwidth (Hz)

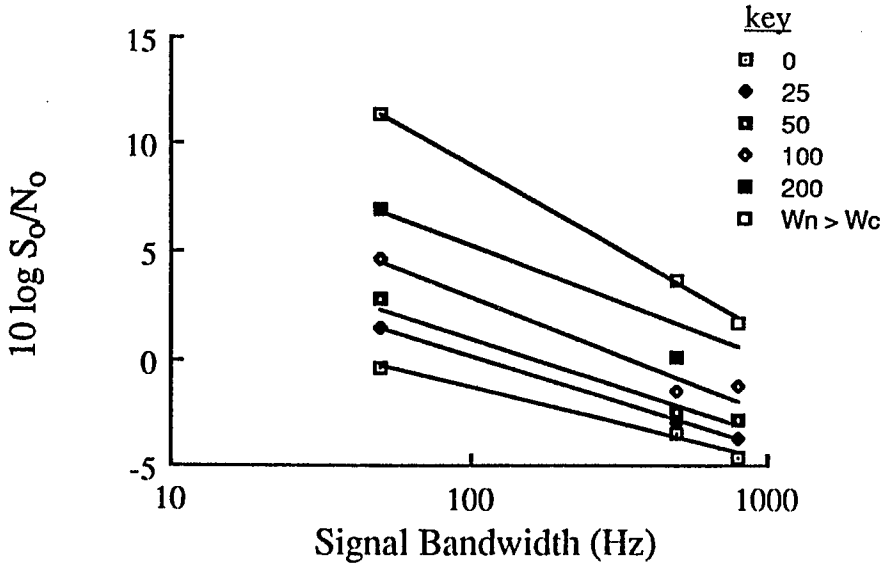
key
0
25
50
100
200
Wn > Wc
15
10
5
0
-5
10
100
1000
10 log S_o/N_o
Signal Bandwidth (Hz)

Table 3.4

Slope of reciprocity function for various values of $W_n - W_s$.

$W_n - W_s$	Slope		
	JA	RB	Mean
0	-0.27	-0.34	-0.31
25	-0.37	-0.44	-0.41
50	-0.43	-0.49	-0.46
100	-0.49	-0.54	-0.52
200	-0.55	-0.52	-0.54
$W_n \geq W_c$ (a)	-0.53	-0.80	-0.67

(a) $W_n \geq W_c$ for all signals.

Figure 3.13

Reciprocity factors as a function of the difference between masker and signal bandwidths ($W_n - W_s$).

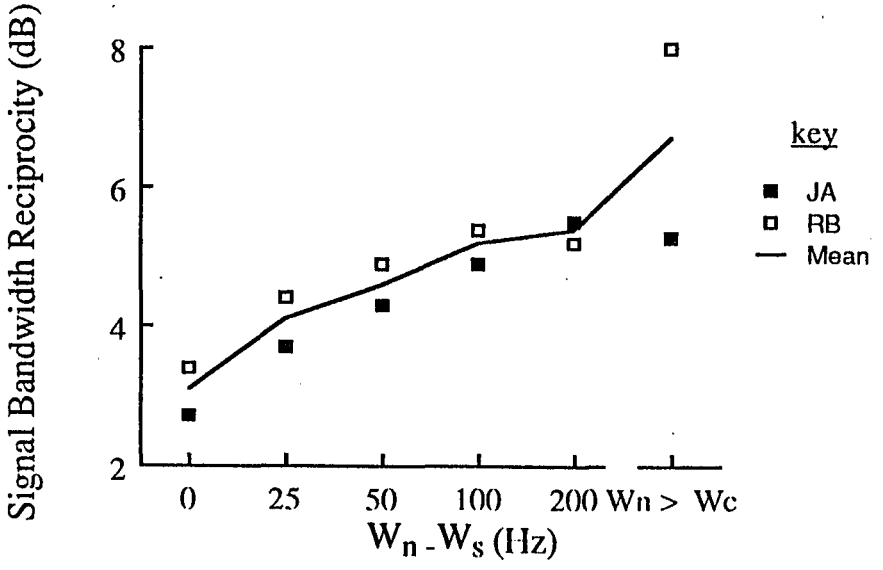
Signal Bandwidth Reciprocity (dB)
8
6
4
2
0
25
50
100
200
Wn > Wc
Wn - Ws (Hz)
key
JA
RB
Mean

on whether or not signal and masker spectra are matched -- a dependency first noted by Schacknow and Raab (1976).

Given that the rate of improvement depends on the relationship between signal and masker bandwidths, we now examine factors which may serve to index the relationship. The factor W_n/W_s is considered first. Thresholds do not change systematically as the ratio is increased. Moreover, at many values of the ratio, thresholds do not decrease monotonically with increasing signal bandwidth. The bandwidth ratio does not seem to be a useful index.

Next we consider the difference between masker and signal bandwidths as an index. Plotted in Figure 3.12 are signal thresholds as a function of signal bandwidth, the parameter being the difference between masker and signal bandwidths ($W_n - W_s$). Threshold values for masker bandwidths not sampled were interpolated from corresponding Fletcher plots (Figures 3.3, 3.4, 3.8 and 3.9). In all cases, line segments reasonably describe performance. It appears that as the bandwidth of the masker differs from that of the signal, changes in signal bandwidth result in greater improvements in performance. The slope of the lines are presented in Table 3.4, and are plotted as a function of $W_n - W_s$ in Figure 3.13. Signal bandwidth reciprocity increases with the difference between masker and signal bandwidths.

3.2.3.3 Slopes of Fletcher Plots

For both narrow- and wide-band signals, increasing masker bandwidth results in elevation of signal threshold. For sub-critical bandwidth signals, the mean slope of the initial portion of the Fletcher plots was 0.88. With supra-critical bandwidth signals (W_s = 500 and 792 Hz), on the other hand, the corresponding mean slope was 3.50.

3.3 Summary

As masker bandwidth is increased, signal threshold is elevated until some critical width is reached. Increases beyond this critical width do not effect the detectability of the signal. Although this is true with both narrow- and broad-band signals, the rate of threshold elevation depends on signal bandwidth.

Estimates of W_c also depend on signal bandwidth. Narrow bandwidth signals are associated with smaller critical widths than wide-band signals, i.e., listeners adjust the bandwidth of the detection process, in accord with the spectrum of the signal.

When the signal to be detected is a sample of noise, performance improves with increasing signal bandwidth. However, the rate of improvement depends on the relationship between signal and masker bandwidths. When signal and masker have the same bandlimits, a log unit increase in bandwidth yields approximately a 3 dB improvement in performance. On the other hand, when masker bandwidth exceeds the signal's critical width, a ten-fold increase in signal bandwidth yields approximately 7 dB of improvement. Rate of improvement seems to be a function of the difference between masker and signal bandwidths.

4. DISCUSSION

In this chapter we will attempt to show that the addition of a simple bandwidth-dependent parameter greatly improves the ability of an energy detector model to fit masking data obtained with narrow-band signals. Thresholds obtained with wide-band noise signals, on the other hand, are poorly predicted by this modified energy-detection scheme. From these findings, we will argue that a complete account of intensity discrimination must include at least two mechanisms: Detection is based on an internal representation of stimulus energy. Stimulus processing imposes bandwidth-dependent variability on the internal test statistic and thus degrades performance. When the signal to be detected is wide-band, an additional mechanism becomes important. This mechanism is thought to be a form of spectral "contrast enhancement."

4.1 Detection of Narrow-Band Signals

4.1.1 Tonal Signal

We are interested in the the effects of bandwidth on the detectability of tones masked by noise. The energy-detection model predicts that the slope of the Fletcher plot is no greater than ½. Slopes reported earlier are steeper (see Table 3.3). Performance departs systematically from predictions based on stimulus energy. On the other hand, substantial evidence exists which supports the argument that stimulus energy is not irrelevant to the prediction of performance.

Given this seeming contradiction, we shall regard the detection mechanism as an energy detector whose performance is degraded by internal processing variability. This is not, of course, a novel approach. Durlach (1963), for example, proposed that (multiplicative) internal noise results from imperfect encoding of stimulus amplitude. Green and Swets (1966) and de Boer (1966) proposed that the detection process is contaminated by additive internal noise. McGill (1967) presented a "hybrid-model"

which considers both external (stimulus) and internal variabilities in order to predict detection performance. In the discussion that follows, we will explicitly link auditory processing variability (i.e., internal noise) to the bandwidth of the stimulus.

We begin by describing the auditory system as consisting of a set of frequency-selective channels. Each channel contains a non-linear device (square-law, for example) followed by an integrator such that a test statistic, Ω_i, is produced which is (at least) monotonic with the energy received by that channel. The index i identifies the channel. We assume that a second stage of processing exists which is capable of summing the outputs of all relevant channels. The output of this second stage is our decision variable and is denoted as L. We define L,

$$L = \sum g_i \Omega_i, \tag{4.1}$$

where g_i may be thought to be the gain of the second stage for a given channel. For simplicity, we will assume that g's are identical within the relevant frequency region and are zero elsewhere. We note that the spectral distribution of g could be made to resemble other filter shapes. However preliminary investigation (see APPENDIX I) suggests that filter shape has a small effect in this task. Implicitly we assume that the monitored frequency band surrounds the test signal and in this context, we interpret traditional critical bandwidth measures as estimating the bandwidth of the second stage. Figure 4.1 summarizes the system described.

Clearly, if the integration of energy within each channel were without error, and the summation of Ω's across channels were perfect, this system would perform as an energy detector. Since real listeners' performance departs systematically from the predictions described earlier, we will attempt to reconcile these difference by introducing bandwidth-dependent variability into the discrimination process.

Figure 4.1

Schematic representation of internal signal processing. See text for details.

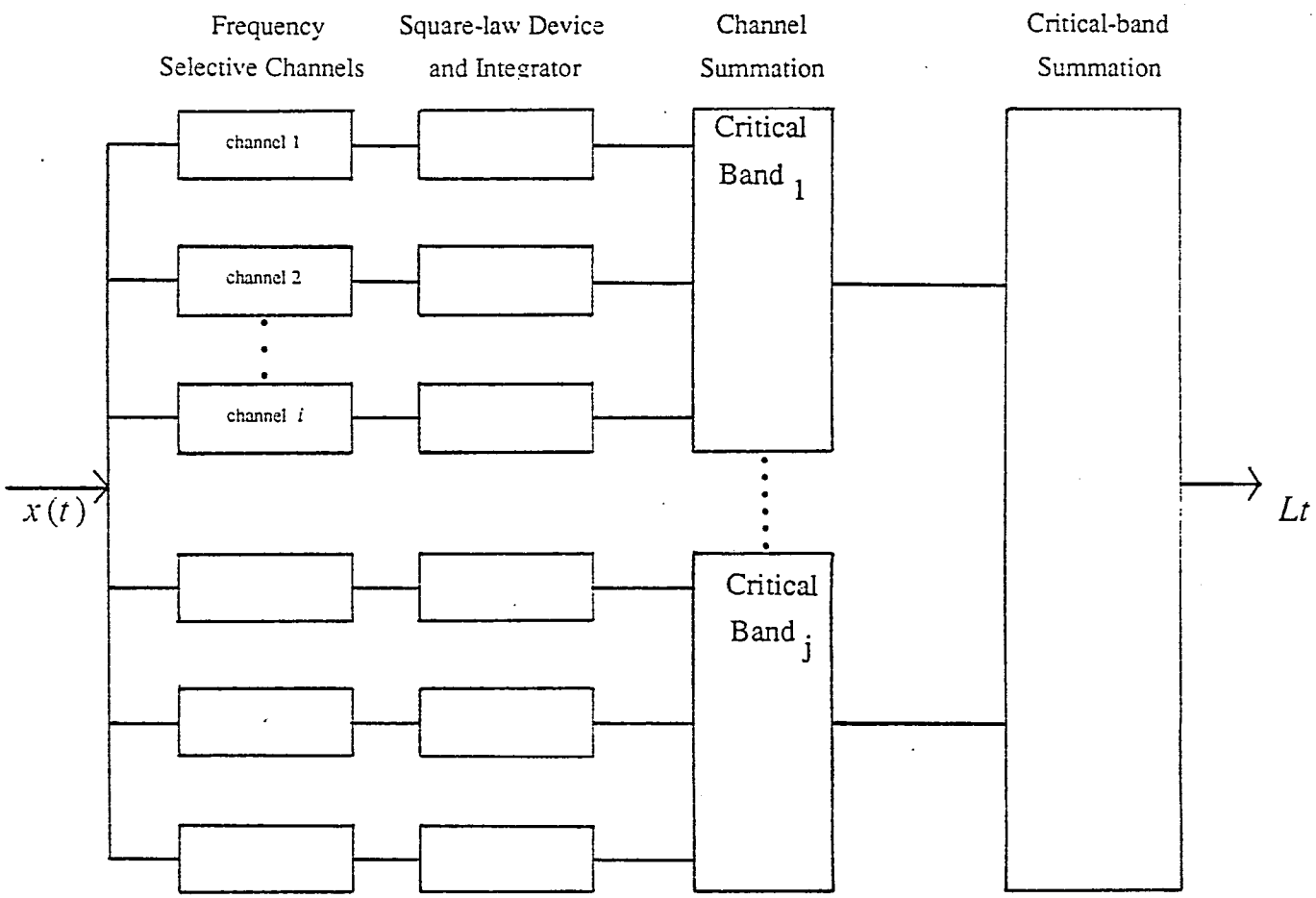

$$\Omega_i = \int_0^T x^2(t)dt \qquad L_j = \sum_{i=1} g_i \Omega_i \qquad Lt = \sum_{j=1} L_j$$

We imagine that the processing of a stimulus is such that, for a given waveform $x(t)$, a value of L is produced proportional to the energy content. That is,

$$E(L|\, x(t)) = c \int_0^T x^2(t)\, dt. \tag{4.2}$$

The scalar c is a constant of proportionality which absorbs the gain function and all units of measurement. The value of L depends only on the energy of the waveform $x(t)$ and not on the presence of the signal in $x(t)$. Watson (1964), showed that listeners' ratings of the likelihood of a signal being present depended strongly on stimulus magnitude and not on the presence or absence of the signal.

4.1.1.1 Description of Internal Noise

In the sections that follow, expressions relating the internal noise to the bandwidth of the masker are developed. This source of variability is then added to the detection equations, thereby degrading performance. Estimates of the (relative) magnitude of internal noise are obtained and then used in calculations of performance. Finally, the predictions of the model are compared to the performance of our listeners.

We begin by describing and developing the characteristics of our internal noise. Let us imagine that an acoustic waveform is reproducible and can be presented repeatedly to a listener. For each presentation, a value of the decision variable, L, is obtained. The transduction of the stimulus, the integration of energy within a channel and the summation of channel outputs (Ω_i's) is considered to be imperfect. Thus, although the waveform is unchanging, a distribution of L's is obtained. This distribution is assumed to be Gaussian. The variable L is considered to be the sum of two components: one component is based on the magnitude of the stimulus which we denote as M; The

second component is the internal noise which we denote as V. Accordingly,

$$L = M + V. \tag{4.3}$$

The variable V is a random variable with zero mean. Recall that $E(L)$ is proportional to the effective energy of the stimulus. It is argued below that the variance of V is proportional to the square of stimulus power evaluated within the passband associated with L.

It is well known that when a tone is masked by white-noise, the signal-to-noise ratio required for constant detectability is largely independent of the spectral density of the masker (Hawkins and Stevens, 1950). That is, Weber's law is known to obtain. This finding implies that the mean-to-sigma ratio of the decision variable is independent of masker level. The energy-detection model satisfies this requirement by treating masker spectral density as a gain factor. The model therefore successfully predicts Weber's law. Normalized detection distances are independent of masker level.

When stimulus variability is experimentally removed (Raab and Goldberg, 1975; Raab and Bernstein, 1979; Siegel, 1979) by employing reproducible noises as the masking waveforms, Weber's law is still obtained. Indeed this is true for narrow- and wide-band signals. Since under these conditions, performance is limited only by internal variability, these findings suggests internal variance is proportional to to the square of masker power (i.e., $(N_0 W_n)^2$). This internal variance is denoted as $Var(V)$ and defined as $k(N_0 W_n)^2$. The scalar k absorbs all preceding constants.

We consider first, the task of detecting a tone in the presence of random noise of bandwidth W_n. Given the independence of M and V, the variance of L is equal to the

sum of external variance ($Var(M)$) and internal variance ($Var(V)$). If

$$E(L) = N_0 W_n T \tag{4.4}$$

then

$$Var(L_n) = N_0^2 W_n T + k(N_0 W_n)^2. \tag{4.5}$$

Similarly, when the tone is added to the noise masker,

$$E(L) = N_0 W_n T + E_s, \tag{4.6}$$

and

$$Var(L_{sn}) = N_0^2 W_n T + 2E_s N_0 + k(N_0 W_n)^2. \tag{4.7}$$

For near-threshold signals, the internal variance is assumed to increase only negligibly upon the addition of the signal. Using the typical assumptions applied to a 2IFC task, the listener reports the observation interval with the larger value of L as the one which contained the signal waveform. It is convenient, therefore, to consider the distribution of differences (i.e., the distribution of the quantity $L_{sn} - L_n$) in deriving estimates of performance. The normalized mean of this difference distribution is given by

$$\bar{L}_{sn} - \bar{L}_n = \frac{E_s}{N_0} \cdot \left[2(W_n T + E_s/N_0 + kW_n^2) \right]^{-1/2}. \tag{4.8}$$

In order to be able to observe the manner in which performance varies with masker bandwidth, we once again fix the mean of this difference distribution at $1/\sqrt{2}$ and solve

for E_s/N_0. Performing the required algebra yields:

$$\frac{E_s}{N_0} = \frac{1+\sqrt{4(W_n T+kW_n^2)+1}}{2}. \tag{4.9}$$

It can be seen that this formulation differs by the term $kW_n{}^2$ from the simple energy-detection model described earlier (see Eq. 1.2). This term represents the variability of the listener's test statistic due to internal processing. Recall that the external variance is proportional to masker bandwidth. Internal variance, in contrast, is proportional to the square of masker bandwidth.

As a consequence of the different proportionalities, we expect that if external variance "swamped" internal variance, threshold would vary approximately with the square-root of masker bandwidth. On the other hand, if internal variance were large compared to the external variance, threshold would vary in nearly direct proportion to masker bandwidth. Stated otherwise, a 10-fold increase in masker bandwidth would result in a threshold increase of 5 dB in the first case and 10 dB in the second case. It should be noted that while the second prediction is similar to the one made by Fletcher's power model, it includes explicit consideration of variabilities in the decision process.

4.1.1.2 Estimation of the Magnitude of Internal Variability

Since the slope of the Fletcher plot depends on the relative contribution of the internal noise, a computer program was written to search parameter space for values of k which best fit the data. Recall that internal variability is equal to $k(N_0W_n)^2$. Slope and intercept estimates from Fletcher plots (see Table 3.3) were used to estimate

Table 4.1

Estimates of k listed by source and listener.

Source of Estimate	Listener		
	JA	RB	Mean
Fletcher Plot			
Tone	.0005	.0015	.0010
50 Hz	.0035	.0075	.0055
Signal Bandwidth Reciprocity	.0007	.0013	.0010
Mean	.0016	.0034	.0025

Figure 4.2

Residual sum of squares as a function of k. The arrows indicate the values of k which minimizes the difference between thresholds predicted from Eq. 4.9 and obtained tonal thresholds. Top: data from listener JA. Bottom: dat from listener RB.

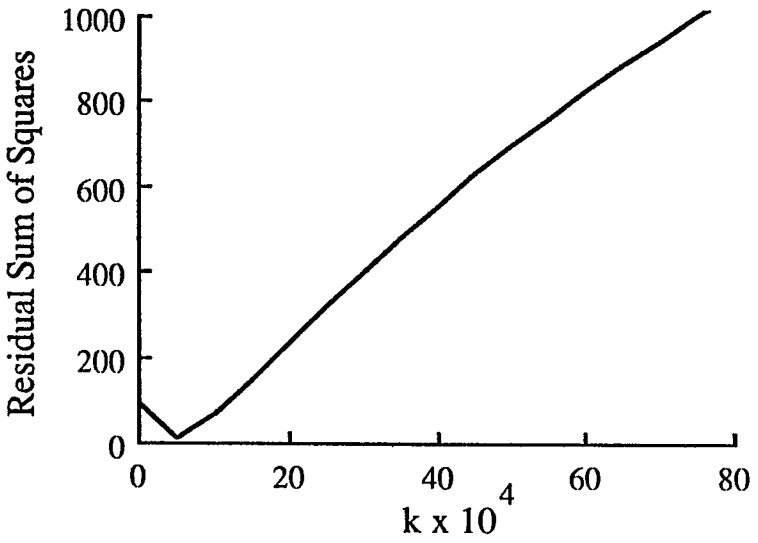
Residual Sum of Squares
1000
800
600
400
200
0
0
20
40
60
80
k x 10^4

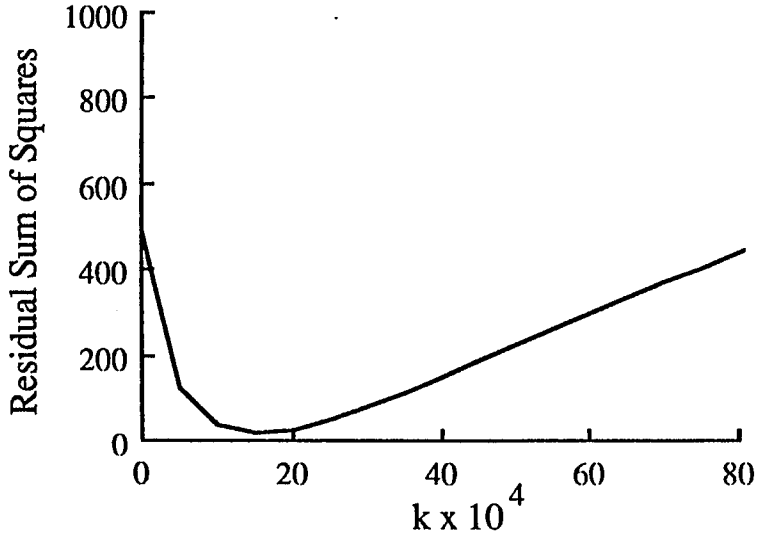
Residual Sum of Squares
1000
800
600
400
200
0
0
20
40
60
80
k x 10^4

Figure 4.3

Tonal threshold as a function of masker bandwidth. Solid triangles are thresholds obtained with sub-critical masker bandwidths. Top: curve is computed from Eq. 4.9 using $k = 0.0005$. Data from listener JA. Bottom: curve is computed from Eq. 4.9 using $k = 0.0015$. Data from listener RB.

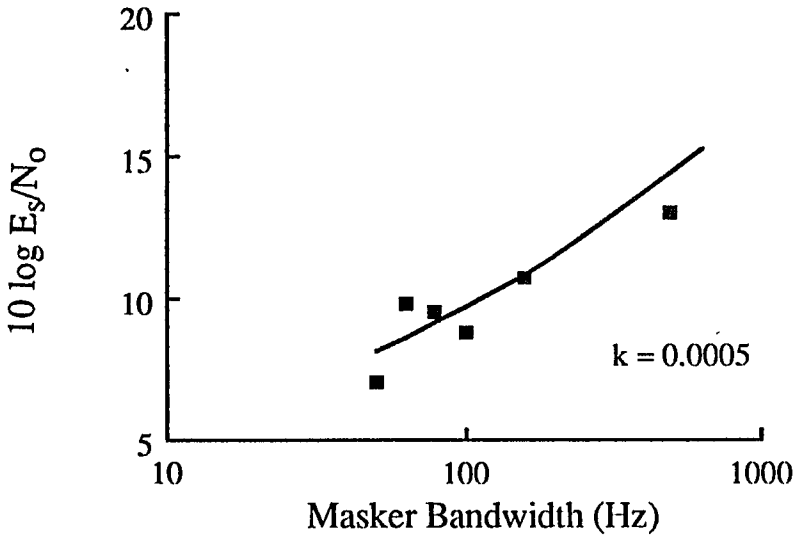
20
15
10
5
10 log E_s/N_o
k = 0.0005
10
100
1000
Masker Bandwidth (Hz)

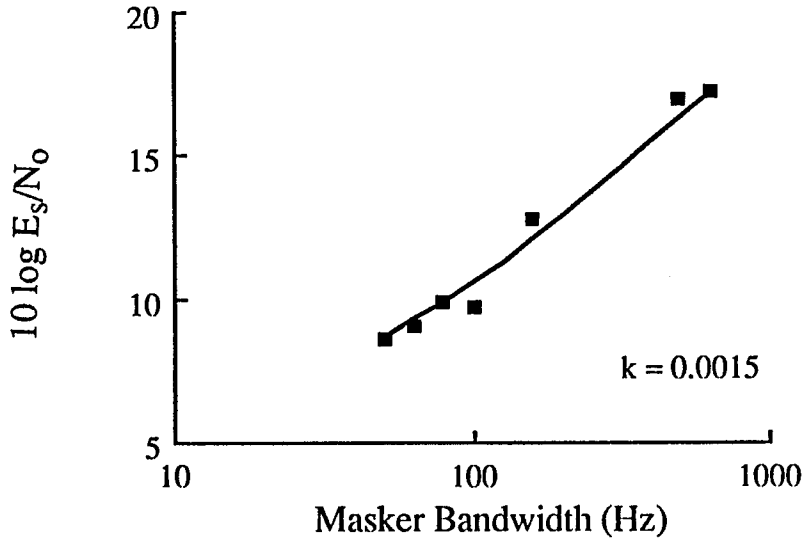
20
15
10
5
10 log E_s/N_o
k = 0.0015
10
100
1000
Masker Bandwidth (Hz)

thresholds (sampling every 10 Hz). These estimates were compared to thresholds computed from Eq. (4.9) for various values of k. Sums of squared-residual differences were computed for each listener at masker bandwidths ranging from 50 Hz to the critical bandwidth (W_c). The value of k which minimized the sum of squared residuals was taken to be as the best estimator of k and is listed in Table 4.1.

Figure 4.2 presents residual sums of squares as a function of k. Residuals for each listener are plotted separately, performance being pooled across levels. Figure 4.3 displays each listener's mean threshold as a function of masker bandwidth and the prediction computed from Eq. (4.9) using the value of k from Table 4.1. It is clear from inspection of Figure 4.3 that the value of k which minimizes the squared residuals also predicts the the first limb of the obtained Fletcher plot. This is true for both listeners.

4.1.2 Narrow-Band Noise Signal

We turn our attention next to the task of detecting a noise signal of bandwidth W_s embedded in a noise masker of bandwidth W_n. Once again, the strategy will be to derive the mean and variance of L conditional on the ensemble from which the stimulus waveform was drawn (n or sn). We then determine the mean and variance of the distribution of differences ($L_{sn}-L_n$). As before, the mean of the normalized distribution is set to equal $1/\sqrt{2}$ and an expression predicting performance is developed.

For the observation containing only the masker, if

$$E(L) = N_0 W_n T \tag{4.10}$$

then

$$Var(L_n) = N_0^2 W_n T + k(N_0 W_n)^2. \tag{4.11}$$

Similarly, for observation intervals containing the signal,

$$E(L_{sn}) = (N_0 + S_0) W_s T + N_0 (W_n - W_s) T \tag{4.12}$$

and

$$Var(L_{sn}) = (N_0 + S_0)^2 W_s T + N_0^2 (W_n - W_s) T + k(N_0 W_n)^2. \tag{4.13}$$

The term $W_n - W_s$ refers to that portion of the masker's spectrum which does not contain the signal. As in the case of tonal signals, the internal variance is increased only negligibly by the addition of near threshold signals. It is implicit that the bandwidth of the masker equals or exceeds that of the signal and that the signal spectrum is always contained within the passband of the masker. The mean of the normalized difference distribution is

$$\bar{L}_{sn} - \bar{L}_n = \frac{S_0 W_s T}{\left[(S_0 + N_0)^2 W_s T + N_0^2 (W_n - W_s) T + N_0^2 W_n T + 2k(N_0 W_n)^2 \right]^{1/2}}. \tag{4.14}$$

We note that if k is set to zero, an expression identical to the Masker-Bandwidth model proposed by Schacknow and Raab (1976) is obtained.

Setting the mean of this distribution to $1/\sqrt{2}$ (for 76% correct decisions) and solving for S_0/N_0 yields

$$\frac{S_0}{N_0} = \frac{1+\left[4(W_n T+kW_n^2)-2\left(\frac{W_n}{W_s}+\frac{kW_n^2}{W_s T}\right)+1\right]^{1/2}}{2W_s T-1}. \qquad (4.15)$$

Consider first, the effect of masker bandwidth on the detection of our narrow-band noise signal (W_s=50 Hz). It is clear that predictions from the model depend on the value of k. As earlier, parameter space was searched for the value of k which best fits the data for this signal. The values from Table 3.3 were used to estimate threshold as a function of masker bandwidth (sampling every 10 Hz). These were then compared to the corresponding thresholds computed from Eq. (4.15). Sums of squared differences were computed separately for each listener at masker bandwidths ranging from 50 to the critical bandwidth (W_c). In Figure 4.4 the sums of squared residuals are plotted as a function of k. The k-value yielding the smallest residual is regarded as the one which best fits the data. In Figure 4.5 the initial limbs of the best fitting Fletcher plots are presented along with the listener's thresholds. Excellent agreement is obtained between data and the model. The best fitting values of k are listed in Table 4.1. We note that for each listener the two signals (tone and 50 Hz noise) yield similar values of k.

4.2 Detection of Wide-Band Signals

4.2.1 The Fletcher Plot

We have seen that our model predicts the slope of the Fletcher plot to be bounded between the limits of ½ and 1 (on log-log coordinates). The slope is determined by the ratio of internal to external variabilities. Our wide-band signals

Figure 4.4

Residual sum of squares as a function of k. The arrows indicate the value of k which minimizes the difference between thresholds predicted from Eq. 4.15 and thresholds of 50 Hz noise. Top: data from listener JA. Bottom: data from listener RB.

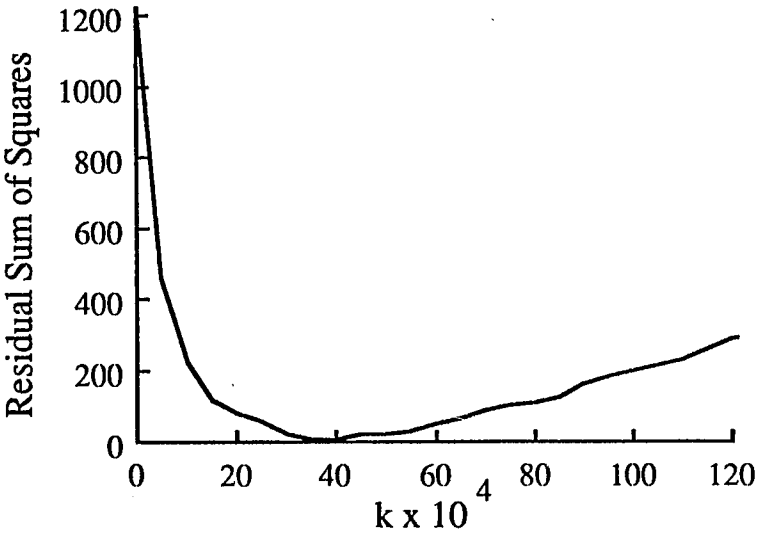
Residual Sum of Squares
1200
1000
800
600
400
200
0
0
20
40
60
80
100
120
k x 10 4

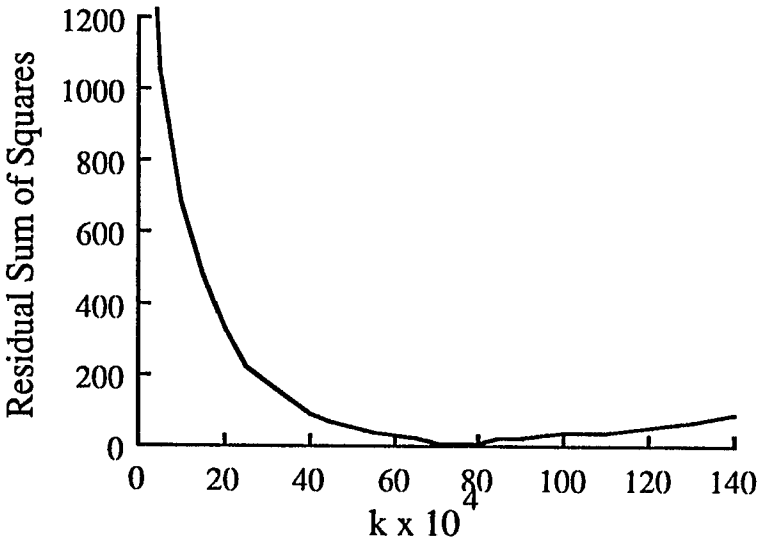
Residual Sum of Squares
1200
1000
800
600
400
200
0
0
20
40
60
80
100
120
140
k x 10 4

Figure 4.5

Threshold of narrow-band noise as a function of masker bandwidth. Solid triangles are thresholds obtained with sub-critical masker bandwidths. Top: curve is computed from Eq. 4.15 using $k = 0.0035$. Data from listener JA. Bottom: curve is computed from Eq. 4.15 using $k = 0.0075$. Data from listener RB.

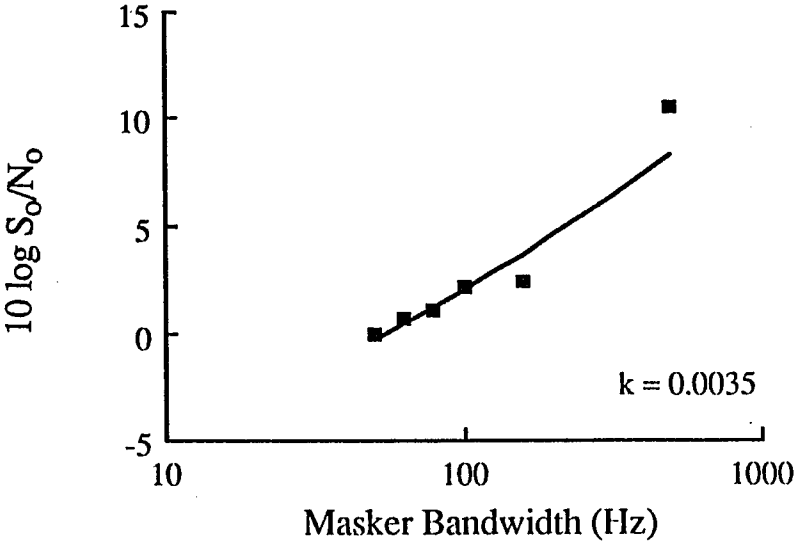
15
10
5
0
-5
10 log S_o/N_o
k = 0.0035
10
100
1000
Masker Bandwidth (Hz)

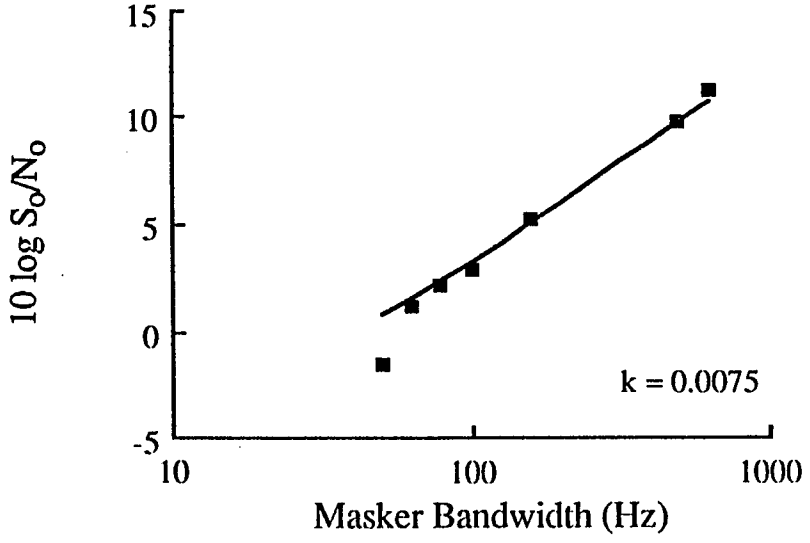
15
10
5
0
-5
10 log S_o/N_o
k = 0.0075
10
100
1000
Masker Bandwidth (Hz)

have slopes that are steeper than unity. As a consequence of these steep slopes, the fit of our model to these data is poor. We defer a discussion of this matter.

4.2.2 Bandwidth Reciprocity

Consider now the effect of increasing signal bandwidth. Recall that when signal and masker had the same bandlimits, the effect of changing bandwidth was small. On the other hand, when the bandwidth of the masker exceeded each signal's critical width, the effect of changing signal bandwidth (W_s) was more pronounced. Reciprocity is estimated by plotting S_0/N_0 as a function of signal bandwidth (log-log coordinates) and determining the slope of the best fitting line.

It can readily be seen that the behavior of our modified energy detection model with respect to signal bandwidth depends on the relationship between signal and masker bandwidths and on the contribution of internal noise to the variance of L. What is not apparent from inspection of Eq. (4.15) is the manner in which masker bandwidths should be equated in order to determine signal bandwidth reciprocities. A bandwidth index that predicts the orderly change in reciprocity for various combinations of signal and masker needs to be determined. The consequences of various measures will now be explored and the one which best fits the data will be designated as the bandwidth index. That done, the effect of internal noise on signal bandwidth reciprocity will be determined.

Let us begin with no internal noise (k=0). In analyzing their model, Schacknow and Raab considered two types of relationships of signal and masker bandwidth. First they examined the situation in which the effective masker bandwidth always matched that of the signal. They noted that this model is identical to the noise-intensity discrimination model of Green (1960). Threshold intensity should vary inversely (approximately) with the square-root of signal bandwidth. This assumption of

matching has two consequences that are not supported by the data. First, the slope of the Fletcher plot should obviously be zero. Second, signal bandwidth reciprocity should be the same irrespective of whether the masker bandwidth equals or exceeds W_s. Schacknow and Raab also considered the case in which the masker is fixed and broadband. Under this assumption, a signal reciprocity of 10 dB was predicted. Unfortunately, they did not consider conditions intermediate between these extremes of signal-masker relationships.

Since signal and masker bandwidths can be varied independently, we seek to index this relationship in a way that is useful for prediction. The ratio (i.e., W_n/W_s) is considered first. This ratio is of course restricted to values equal to or greater than 1. Plotted in Figure 4.6, are the reciprocities evaluated for signals employed in this study as a function of W_n/W_s. The reciprocity (evaluated from W_s = 50 to W_s = 792) is predicted to be 6 dB when W_n/W_s=1 and reduces slightly when the ratio is increased. Our data show the opposite pattern; when $W_n/W_s = 1$ the reciprocity is less than that obtained when $W_n/W_s>1$. Moreover, reciprocity was not a monotonic function of the bandwidth ratio.

The bandwidth difference (W_n-W_s) is considered next. Plotted also in Figure 4.6 are the reciprocities computed from Eq. (4.15) as a function of W_n-W_s. It is clear that the predicted reciprocity increases as the bandwidth difference increases from zero. These theoretical values are, however, everywhere larger than the corresponding empirical values (see Figure 3.13).

The reciprocity function is affected by internal variability. In Figure 4.7 are plotted the reciprocity functions (i.e., reciprocity as a function of W_n-W_s) for various values of k. In general, it can be seen that the addition of internal noise results in reductions in

Figure 4.6

Bandwidth reciprocity as a function of: a) the ratio of masker and signal bandwidth and b) the difference between masker and signal bandwidths. Thresholds computed from Eq. 1.8. Signal bandwidths of 50, 500 and 792 Hz were used to determine reciprocity factors.

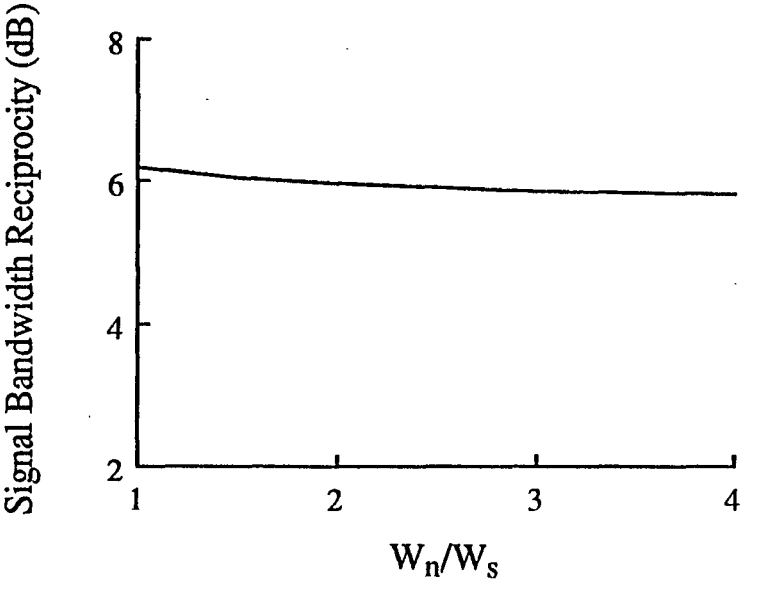
Signal Bandwidth Reciprocity (dB)
8
6
4
2
1
2
3
4
W_n/W_s

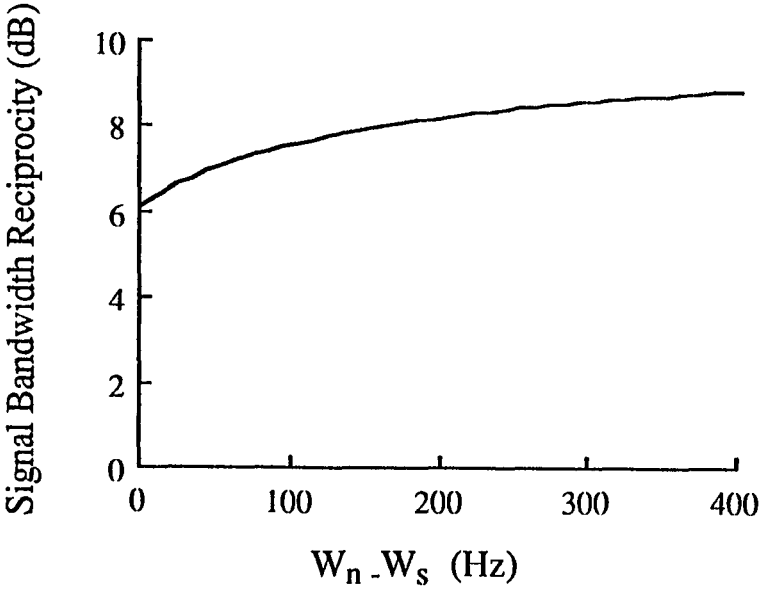
Signal Bandwidth Reciprocity (dB)
10
8
6
4
2
0
0
100
200
300
400
$W_n - W_s$ (Hz)

Figure 4.7

Bandwidth reciprocity as a function of the difference between masker and signal bandwidths (W_n–W_s). Thresholds were computed from Eq. 4.15. Signal bandwidths of 50, 500 and 792 Hz were used to determine reciprocity factors. Top: reciprocities for various values of k. Bottom: comparison of empirically derived factors replotted from Figure 3.15 and the theoretical function based on k =.001.

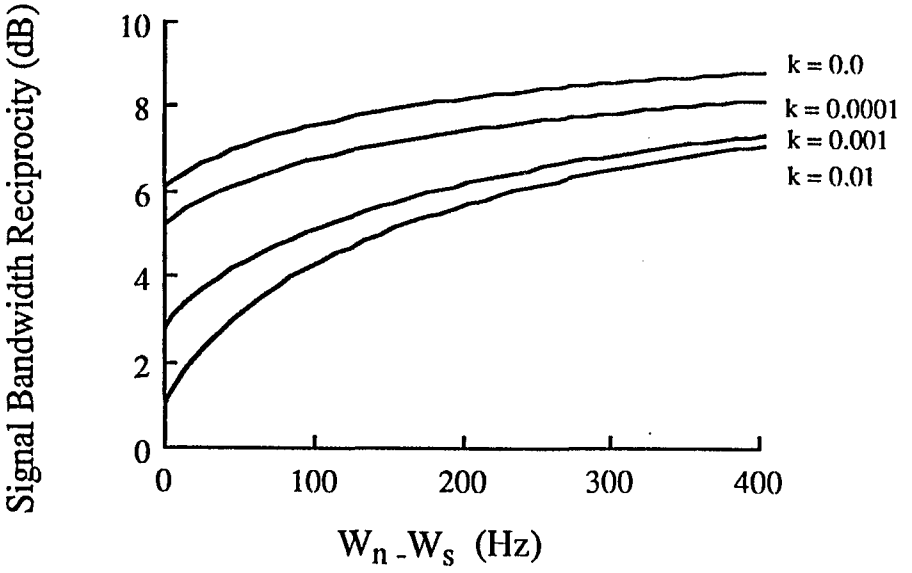
Signal Bandwidth Reciprocity (dB)
10
8
6
4
2
0
0
100
200
300
400
k = 0.0
k = 0.0001
k = 0.001
k = 0.01
$W_n - W_s$ (Hz)

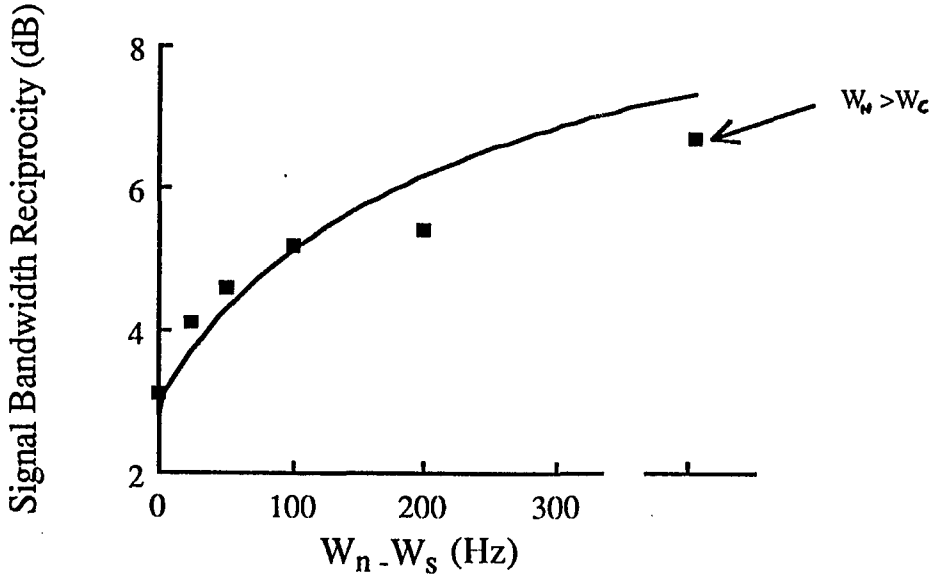
Signal Bandwidth Reciprocity (dB)
8
6
4
2
0
100
200
300
$W_w > W_c$
$W_n - W_s$ (Hz)

in reciprocity. This is true for all values of $W_n - W_s$, but the effect is more pronounced for small values of $W_n - W_s$. The value of k which best predicts the obtained reciprocity function was determined as follows: The reciprocities for the condition of zero bandwidth difference were computed for various values of k and compared to each listener's corresponding empirical estimate. The value of k which yielded the empirically determined reciprocity factor was selected. These k-values are listed in Table 4.1. The reciprocity function based on the average of these k's (k=.001) is plotted in bottom panel of Figure 4.7 along with the corresponding empirical factors. Observed and theoretical factors are similar. Moreover, these k-values are close to those determined from narrow-band Fletcher plots (see section I).

We have now seen that the addition of a simple bandwidth-dependent source of variability dramatically reduces several discrepancies between theory and performance. Searches of several parameter spaces for different experimental conditions yielded similar estimates of k (see Table 4.1). Estimates from different subjects are also similar. Performance in the tasks studied is conveniently summarized by our modified energy detector.

4.3 The Ratio of Internal Variance to Total Variance

Given that our internal noise is bandwidth-dependent, it follows that the proportion of variance of the decision variable that is due to internal processing changes with bandwidth. As a first approximation, let us consider the variance of L for observation intervals containing masker alone. Recall that the external (stimulus) variance is given by

$$N_0^2 W_n T \tag{4.16}$$

and the internal variance is given by

$$k(N_0W_n)^2. \tag{4.17}$$

The ratio of internal to total variance is, accordingly,

$$\frac{k(N_0W_n)^2}{N_0^2W_nT+k(N_0W_n)^2} \tag{4.18}$$

which reduces to

$$\frac{kW_n}{T+kW_n}. \tag{4.19}$$

For example, if we assume that $k = .001$ and T = 0.1 sec, it can be seen that when W_n = 100 Hz the ratio is ½. On the other hand, when W_n=1000. the ratio becomes 0.91. Stated otherwise, for the narrow-band masker of this example, internal variance was equal to external variance. For the wide-band example, internal variance was 10-times as great as external variance. We note that this relationship is consistent with the observations of Raab and Goldberg (1975). In their study, the discriminability of noise bursts with and without energy fluctuations was determined. Estimates of internal-to-total variability were then obtained by two independent methods which yielded comparable results. Raab and Goldberg showed that for a fixed duration signal the proportion of variance that is internal increased with bandwidth (see their Table VI). Precisely this relationship is predicted by our model.

4.4 The Slope of the Fletcher Plot for Wide-Band Signals

We return now to a discussion of the form of the Fletcher plot obtained with supra-critical bandwidth (W_s=500 and 792 Hz) signals. Recall, that the threshold increased with masker bandwidth until some critical width (W_c) was exceeded. Threshold then became independent of further increases in W_n. The rate of threshold

increase exceeded (a) the rate observed with narrow-band signals (tone and W_s=50 Hz) and (b) the rate predicted by our model. It is this issue that we address next.

Wide-band signals yielded slopes greater than 2.0. These steep slopes are consistent with the data presented by Schacknow and Raab (cf. their Figures 7 -10) and with data obtained by Bernstein and Baruch (1977) in a study preliminary to the present investigation. We shall see that these slopes require an additional mechanism to be active.

4.4.1 Effective Signal Bandwidth

Schacknow and Raab (1976) found that adding noise outside the passband of a wide-band signal resulted in a performance decrement. This effect was found for signals ranging in bandwidth from 100 to 3000 Hz. Precise estimation of the slopes of the Fletcher plots was not possible because of the coarse spacing of masker bandwidths. It is clear however, that the slopes typically exceed unity. It is noteworthy that "critical bandwidths" increased with signal bandwidth. This trend is also evident in the data from the present study (see Table 3.3). In addition Schacknow and Raab found that signal bandwidth reciprocity was less when signal and masker were filtered together (i.e., homogeneous in bandwidth) than when masker bandwidth exceeded that of the signal (heterogeneous in bandwidth).

In the model presented by Schacknow and Raab, the dependence of reciprocity on homogeneity (versus heterogeneity) of bandwidth was related to the "steep" slope of the Fletcher plot. The effective bandwidth of a signal differs systematically from its half-power bandwidth (HPB). The difference depends on W_s and on the similarity of signal and masker bandlimits.

Stimulus waveforms, in their study, were derived by passing a (wide-band) noise through analog filters. A consequence of this is that energy is present outside the

nominal (half-power) passband. The existence of these out-of-band components causes signal detectability to depend on bandwidth homogeneity. It turns out that HPB and effective bandwidth are similar for the heterogeneous conditions. When bandwidths are homogeneous however, the effective bandwidth of a signal is greater than its HPB. The difference between these measures is least when the bandwidths are large.

Consider the consequences of this dependency. For a given change in HPB, the change in effective bandwidth depends on the heterogeneity of signal and masker. It follows then that signal bandwidth reciprocity depends on heterogeneity. Since the change in effective bandwidth would be less in homogeneous conditions than in heterogeneous conditions, signal bandwidth reciprocity should be smaller when signal and masker are homogeneous. Consider the effect of the preceding on the slope of the Fletcher plot. Increasing masker bandwidth results in an increase of heterogeneity of bandwidth. A consequence of this increase is that effective signal bandwidth decreases. Detectability should decline both because of the increase in masking energy and because of the decrease in effective signal bandwidth. The slope of the Fletcher plot should be steep.

Effective bandwidth was thought by Schacknow and Raab to differ from HPB for two reasons. First, it was argued that HPB was an inadequate specification since it ignored out-of-band components. Second, and more important, they postulated that neural compression could result in partial "prewhitening" when $W_n = W_s$. This would cause frequency components near the center of the passband to be weighted less heavily than less intense components at the band edges. Such a process would result in a stimulus whose effective bandwidth is greater than that specified by HPB.

Moschetto (1978) reasoned that if prewhitening were responsible for the increased discriminability of signals in homogeneous conditions, then performance should vary

with the intensity of out-of-band components. That is, threshold should vary with the rate of off-frequency attenuation (i.e., with the slope of the filter skirt). To test this prediction, performance in a noise intensity discrimination task was compared for stimuli matched in HPB and spectrum level but differing in the rate of off-frequency attenuation (24 vs. 96 dB/octave). Consistent with the notion of prewhitening was the fact that thresholds obtained with the 24 dB/octave filter were better than those obtained with the steeper filter skirt. However, the differences were small -- averaging less than 1 dB. The fact that the effect of attenuation rate is small suggests that prewhitening does not provide a complete explanation for the results obtained by Schacknow and Raab. Moreover, inasmuch as our noise-bands had nearly rectangular spectra, effective bandwidth should be nearly the same as the nominal bandwidth for both homogeneous and heterogeneous conditions.

4.4.2 Energy Splatter

Steep slopes (of Fletcher plots) were reported by Spiegel (1981). The signals in his study were pure tones. Because conditions in that study were identical to those employed in an earlier work (Spiegel, 1979) except for differences in rise/fall times, Spiegel suggested that steep slopes might be due to listener strategy. The average slope reported in Spiegel's first study was 0.7 which is consistent with the results obtained in the present research. Spiegel explained the differing results obtained in his two studies by suggesting that when the masker is narrow band, threshold could be improved by listening "off-frequency" (cf. Leshowitz and Wightman, 1971). That is, the listener monitors frequency regions outside of the masker spectrum for the presence of (splattered) signal components. The decreased rise/fall times in the second study would result in relatively more energy "splatter" than present in the first study. Narrow band maskers in the second study should be less effective than in the first study. Increasing the masker bandwidth reduces the advantage of such "off-frequency" listening. Wide

band maskers would be equally effective in both studies. The slope of the Fletcher plot is steep in the second study because of the (bandwidth-dependent) change in listener's strategy.

The signals in the Spiegel studies were always shorter in duration than the maskers (0.1 and 2 seconds, respectively). Regions of improved signal-to-masker ratio existed because of the difference in signal and masker duration. In the present study however, signal and masker were always gated identically. This ensured that signal-to-masker ratios were everywhere uniform. Off-frequency listening would not be an advantageous strategy. Furthermore it seems unlikely that this strategy would be employed only with wide-band signals. In the present study, slope estimates from narrow-band signals are less than those obtained from wide-band signals. Changes in listener strategy do not seem to be a useful explanation for the effects obtained.

The steep slopes obtained with wide-band signals cannot be accounted for by a process of prewhitening or by bandwidth-dependent listening strategies. In the section that follows we argue that these steep slopes reflect the operation of a type of "contrast enhancement" mechanism.

4.4.3 Enhancement of Spectral Contours

We began this chapter by describing the auditory system in terms of frequency selective channels. A decision variable L was defined as the summed output of the channels contributing to a given critical band. The gain of all channels within a critical band was assumed to be equal. When the signal was narrow with respect to the critical bandwidth, the listener based his responses on inspection of the value of L_j from the critical band surrounding the signal. The subscript j is introduced to identify the band. Clearly, when the signal is wider than one critical band, the listener must form a decision variable by summation of L's from the critical bands surrounding the signal.

We denote this variable as Lt and define

$$Lt = \sum L_j. \tag{4.20}$$

In this context, we interpret W_c as the bandwidth region contributing to the formation of Lt. It is assumed that the bands included in the summation depend on the bandlimits of the signal. That is, W_c is thought to increase with W_s, and, in general, W_c will exceed W_s.

We now introduce the additional assumption that the gain of a given band depends, in part, on the amount of excitation present in adjacent bands. The excitation of a band is primarily determined by the spectral characteristic of the masker. The gain of a given band declines with excitation in adjacent bands. This form of "lateral suppression" results in greater gain in the critical bands at the edges of a masker than at its center. The distribution of gains (across bands) resulting from a wide band rectangular masker would be U-shaped. The relationship between input spectrum and internal spectrum is depicted schematically in Figure 4.8. This type of interaction is similar to mechanisms invoked in accounts of such visual phenomena as Mach bands and Cornsweet edges. It is clear that with the stimulus processing architecture described above, the distribution of gains would not affect the slope of the Fletcher plot obtained with narrow-band signals. The situation is more complex when the signal is wide-band.

We consider first the effect of the gain distribution when signal and masker have matched bandlimits (i.e., are homogeneous). It is readily demonstrated that the signal-to-masker ratio is independent of the details of the gain distribution. The only requirement is that $g_j \neq 0$. The reader is reminded that Houtgast (1972) argued that

Figure 4.8

Pictorial representation of stimulus spectrum and internal spectrum. The transformation is the result of the gain function (see text). On the left, signal and masker bandwidths are equal. Signal-to-noise ratio is not changed by the transformation. On the right, masker bandwidth exceeds signal bandwidth. The region of no signal is indicated with stripes. Signal-to-noise ratio is reduced by the transformation.

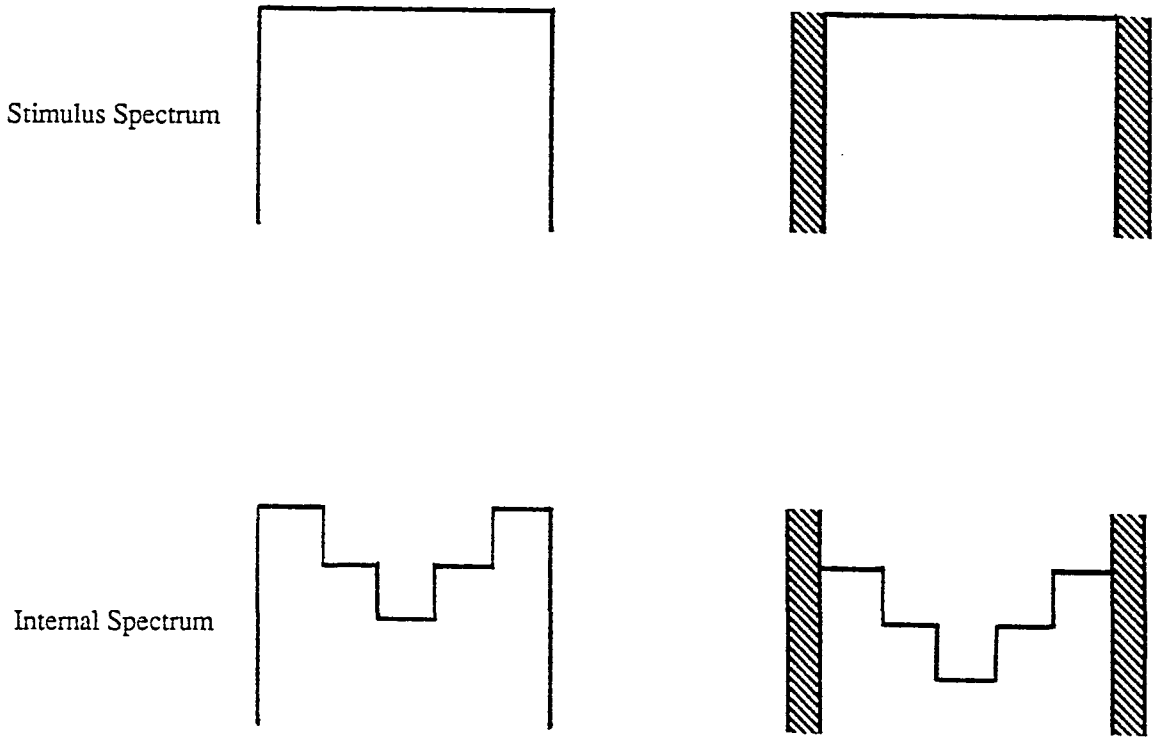
Stimulus Spectrum
Internal Spectrum
$W_n = W_s$
$W_n > W_s$

lateral suppression effects are not observed in simultaneous masking (homogeneous in time) because suppression mechanisms change only gain leaving signal-to-masker ratio constant. The situation is different with temporal masking (i.e., heterogeneous in time) since the gain of the system during the presentation of the masker is different from the gain during presentation of the signal. Signal-to-masker ratio is changed by suppression. In an analogous fashion the situation is also different when the bandwidth of the masker exceeds that of the signal since the gain is not uniform across region of the masker with and without the signal.

It can be appreciated from inspection of Figure 4.8 that the addition of a small amount of masker energy in frequency regions flanking the signal would result in a substantial increase in the internal representation of the energy of the masker. The gain of the bands at the masker edges is high compared to the gain at the center of the passband. It is as if the spectral density of the portion of the masker flanking the signal were greater than at the center of the passband. Performance would be degraded beyond the amount of additional masking expected from the increment of masking energy. A small amount of masking energy added to the band edges results in a large increment in masking. A consequence of the dependency of the spectral distribution of gain on the the masker spectrum is that maximum gain is always in the bands located at the masker bandlimits and the minimum gain is always at the center of the passband. It follows from these considerations that the slope of the Fletcher plot would be steeper with wide-band signals than with narrow-band signals. These are the results obtained.

We note that the dependency of the gain function on the masker spectrum results in poor performance with wide-band signals. This may be so because the task of detecting a wide-band signal embedded in a still wider band masker is one with little utility. However, it should be noted that the representation of the masker bandlimits are enhanced by this form of processing. The auditory system may be designed to

determine the spectral contours of wide band stimuli. The poor performance observed in heterogeneous conditions with wide-band signals reflects the activity of a (spectral) contrast enhancement mechanism. This mechanism may enhance the identification of the edges of a wide-band stimulus at the expenses of degraded performance in heterogeneous intensity discrimination.

5. APPENDICES

5.1 APPENDIX I -- Noise-Energy Distributions

5.1.1 The Gaussian Assumption

The performance of a detector depends, in part, on the shape of the decision variable's distribution. For stimulus parameters yielding a large number of degrees of freedom (df), the Central Limit theorem suggests that stimulus energy is distributed normally. We are, however, interested in predicting the results of band-widening experiments. Of concern are those situations where stimulus parameters yield small numbers of df, and where the Gaussian assumption may not be tenable (Spiegel, 1981). It is therefore worthwhile to examine the magnitude of error introduced by the assumption of normal distributions for conditions with few df.

In the frequency domain, the noise maskers may be represented with a discrete Fourier series. Each of the WT spectral components may be envisioned as a pair of orthogonal vectors with magnitudes that are normal deviates. The power of each component is proportional to the sum of 2 squared unit-normal deviates. Hence the power of each component is proportional to a χ^2 variate with 2 df. The constant of proportionality is the spectral density (N_0) of the noise. Summing the power of all components results in a test statistic proportional to a χ^2 variate with $2W_nT$ df.

The addition of the tone to the noise may be modeled as the addition of a vector of fixed magnitude and random phase to the component at the signal frequency. The power of this component is proportional to a non-central χ^2 variate. The non-centrality parameter (λ) equals $2E_s/N_0$ (Green and Swets, 1974). Summing the power of all components during the signal interval results in a quantity proportional to a non-central χ^2 variate with $2W_nT$ df. Although it is known that the proportion of correct decisions for a 2IFC task is given by the tail area of an non-central F distribution (Green and

McGill, 1970), simple expressions for the difference distribution are not available. Thus, it is not known whether Eq. (1.2) is accurate for conditions with few df. To asses the accuracy of Eq. (1.2), a series of Monte-Carlo simulations were performed.

A program was written to obtain for each of 10000 "stat-trials" the "waveform-power" in both an interval containing masker alone (n-interval) and an interval containing tone plus masker (sn-interval). For the n-intervals, the power of each component was determined by drawing two independent deviates from a unit-normal distribution. This was repeated WT times. Each normal-deviate represents the amplitude of one vector. The "power" of a component was obtained by squaring each deviate and computing the sum of the two squares. Since the sum of squared unit-normal deviates is distributed as χ^2, the "power" in this half of the trial had the appropriate density. The number of df equaled twice the number of components, as is required by the model. For the intervals containing the tone, the "power" was constructed in a similar fashion except that prior to squaring, a constant (which equaled the RMS voltage of the signal) was added to one vector of the central component. The "power" of this component is distributed as non-central χ^2. The percentage of trials where "power" of the tone plus masker exceeded the "power" of masker alone is the percent correct decisions.

Signal levels supporting 76.04 percent correct decisions were computed from Eq. (1.2) for 6, 14 and 22 df (i.e., for maskers with 3, 7 and 11 components). The simulations yielded 76.68, 76.39 and 76.27 percent correct decisions, respectively. We conclude that assuming a Gaussian density does not introduce serious error for conditions yielding as few as 6 df. It is noteworthy that even closer agreement between the Gaussian model and simulation was obtained with more df -- a finding consistent with the Central Limit theorem.

5.1.2 Effects of 'Realistic Filtering'

In our analysis thus far, we have assumed that all components of the noise contribute equally to the masking of the signal. This is equivalent to assuming that the listener places an auditory filter with a rectangularly shaped passband at some stage of processing prior to the detector. It is certainly true, however, that the passband of the listener's filter is not rectangular. With this in mind, we now determine the effects of more "realistic" filtering on the form of the Fletcher plot.

Patterson and Henning (1977) have shown that the slope of the Fletcher plot is reduced when the auditory filter is assumed to be "tuned" (double exponential) rather than rectangular. In their derivation the decision variable was assumed to have a Gaussian density. It seems worthwhile to extend this examination to another type of tuned filter.

We assume that the transfer function (of power) is given by

$$e^{\frac{-x^2}{2}}; \qquad x = \frac{f - f_c}{\sigma} \tag{A1.1}$$

(see for example, Houtgast 1974, 1977; Patterson 1976). The discrete nature of our noise representation may be exploited by applying the filter weights to each component separately. For simplicity we require WT to be an odd integer. Thus for the interval containing only the masker,

$$Var(\Omega_n) = 2 \sum_{i=\frac{1-WT}{2}}^{\frac{WT-1}{2}} e^{\frac{-X_i^2}{2}}; \qquad X_i = i\,\Delta x. \tag{A1.2}$$

and for the interval containing the signal plus masker,

$$Var(\Omega_{sn}) = 2 \sum_{i=\frac{1-WT}{2}}^{\frac{WT-1}{2}} e^{\frac{-X_i^2}{2}} + 4\lambda; \qquad X_i = i\Delta x. \tag{A1.3}$$

Assuming that the signal is added to the center of the passband and setting the normalized mean of the difference distribution to $1/\sqrt{2}$ yields

$$\frac{S_0}{N_0} = 2 + \left[\frac{8 \sum e^{\frac{-X_i^2}{2}} + 4}{2} \right]^{1/2}. \tag{A1.4}$$

Plotted in Figure A1.1 are the predicted thresholds as a function of df, the parameter being the spacing of frequency components (Δx). Clearly these functions are similar to each other. We note that the slopes of these plots are less steep than that obtained with a rectangular bandpass filter. This finding is similar to the result calculated by Patterson and Henning (see their Figure 5) and extends their analysis to another type of tuned filter.

In order to confirm that under these conditions of filtering our decision variable is still approximately Gaussian we return once again to simulation. This time however, prior to summing, we scale the contribution of each component by the filter weight. Signal levels were determined from Eq. (A1.4) for 6, 14 and 22 df and Δx of 0.10. The percent correct decisions were 76.63, 76.22 and 76.27 respectively. Even with a masker whose spectral density is not uniform, the decision variable is distributed in nearly Gaussian fashion.

Figure A1.1

Threshold as a function of log df. The internal filter is assumed to be non-rectangular (see text). Thresholds are computed from Eq. A1.4. The parameter is the density of spectral components (Δx).

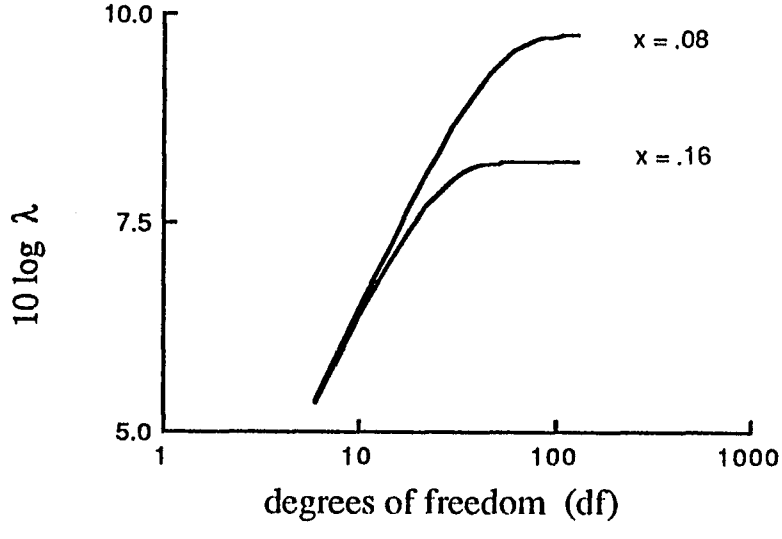
10.0
7.5
5.0
10 log λ
x = .08
x = .16
1
10
100
1000
degrees of freedom (df)

5.2 APPENDIX II -- Synthesis of Noise Waveforms

5.2.1 The Number of Components Required

Noise may be represented by

$$C \sum_{n=1}^{N} \cos (2\pi ft - \theta_n) \qquad \text{(A2.1)}$$

where θ is a random phase angle distributed uniformly over the range $0, 2\pi$ and C is a constant (see Rice, 1954 section 2.8). We have found it convenient to employ this representation as the basis of synthesis.

5.2.1.1 Distribution of Instantaneous Amplitudes

If we have an ideal noise source generating a voltage across a 1 ohm resistor, instantaneous amplitude is distributed in a normal fashion. It is desirable that our synthetic noise also have this characteristic. If we represent the noise waveform as the sum of sine waves with random starting phases, it becomes necessary to determine how many components are needed. The Central Limit Theorem predicts that as the number of components (N) approaches infinity, the resultant distribution of instantaneous amplitudes approaches the normal.

For a single component with unit amplitude, the population $x = \cos \theta$ has the distribution curve depicted in Figure A2.1 and given by

$$f(x) = \frac{1}{\pi (1-x^2)}. \qquad \text{(A2.2)}$$

The distribution is symmetrical but bimodel and hence departs in kurtosis from the normal distribution. One measure of kurtosis, B_2, is defined as the ratio of the fourth moment to the square of the second moment. The second and fourth moments of the distribution depicted in Figure A2.1 are ½ and 3/8, respectively. B_2 is therefore 1.5 (Slack, 1946). The kurtosis of a unit-normal distribution equals 3. We expect that the

Figure A2.1

Distribution of instantaneous amplitude (absolute value) for a unit sinusoid.

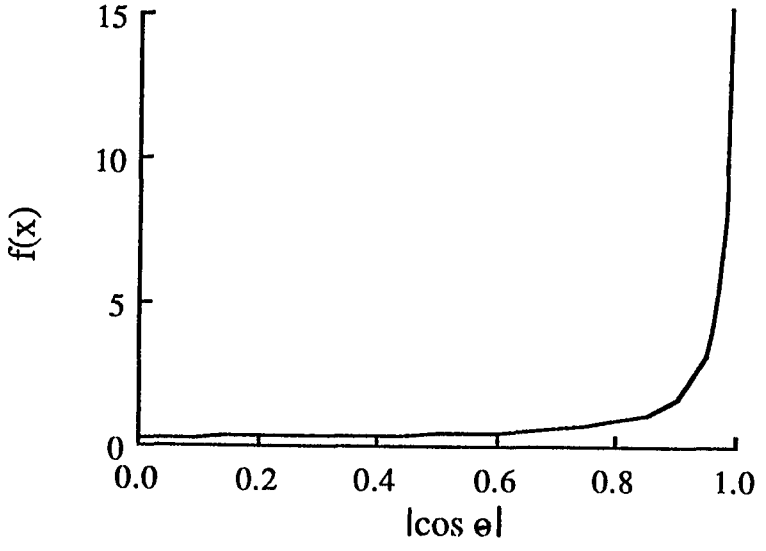
15
10
5
0
f(x)
0.0
0.2
0.4
0.6
0.8
1.0
|cos θ|

value of B_2 will increase from 1.5 (N = 1) and approach 3 when the number of components is sufficiently large so that the distribution of instantaneous amplitudes is nearly Gaussian.

When N components having equally likely phase angles are combined at random, the resultant amplitude probability distributions are independent of the frequency of oscillation (Slack, 1946). The distribution of amplitudes can be simulated by randomly sampling the sine function in the interval $0, 2\pi$. A computer program was written which generated 2000 samples each of size N (N = 1,2,3,.., 50,100,150,...350). For each component in each sample, a random phase angle was determined, and the value of $\sin \theta$ was computed. For the resultant amplitude distributions, the statistic B_2 was then computed.

Figure A2.2 presents a plot of B_2 as a function of sample size. We note that: (1) For $N = 1, B_2$ equaled 1.498, which is consistent with the parameter value of 1.5. (2) In the region beyond $N = 15, B_2$ approaches an asymptote near 3, the parameter of the normal distribution. (3) The change of B_2 with sample size is consistent with the formula, $B_2 = 3–3/2N$, derived by Slack (1946). The solid curve in Figure A2.2 represents a plot of that function. It is also noteworthy, that Slack had concluded that the amplitude distribution for sample sizes exceeding 10, is well approximated by the normal distribution except for extreme tail regions. That this is so, may be demonstrated by recalling that the probability of x exceeding N is zero; whereas, for the normal distribution, x lies between $-\infty,\infty$.

It was decided that at least 50 components would always be employed in the synthesis of noise-bands. This ensured that the noise-amplitude distributions would be very nearly Gaussian. Moreover, the approximation would not be noticeably improved when sample size exceeds 50.

Figure A2.2

B_2 as a function of sample size. Data points are from simulation (see text). Solid curve represents the theoretical function derived by Slack (1946).

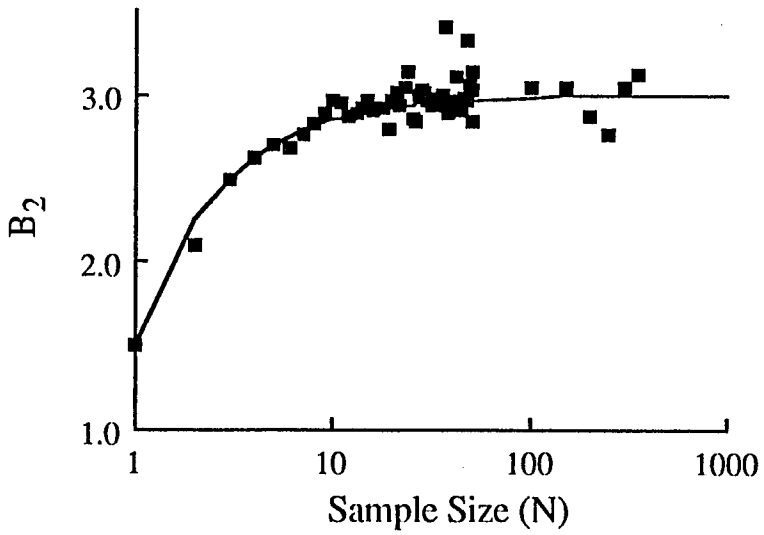
3.0
2.0
1.0
B_2
1
10
100
1000
Sample Size (N)

5.2.1.2 Distribution of Energy

We are interested in representing a waveform, $n(t)$, over the finite time interval $(0, T)$ and we require that the quantities,

$$\hat{E} = \sum n_i^2 \Delta t$$

and

$$E = \int n^2(t)\, dt \tag{A2.4}$$

be distributed in a similar fashion. Representation of the waveform by a discrete Fourier series suggests that we need to employ $2WT$ spectral components, where W and T are the bandwidth and duration of the waveform, respectively. Thus, from considerations of the amplitude distribution of $n(t)$ and of the ensemble distribution of E, we synthesize our noise bands with N spectral components, where N was determined by the rule;

$$\begin{array}{ll} N = 50; & 2WT < 50, \\ N = 2WT; & 2WT \geq 50. \end{array} \tag{A2.5}$$

5.2.2 Sampling Considerations

5.2.2.1 Time Domain Sampling

Sampling theorems suggest that a waveform $n(t)$ may be reconstructed from the values of the waveform at discrete, equally spaced intervals in time. Such a sample-and-hold procedure yields a spectrum which is the convolution of the input spectrum and the Fourier transform of the gating function. For the uniform time window employed; the gating function $G(t)$

$$\begin{array}{ll} = 1; & \dfrac{-T}{2} < t < \dfrac{T}{2}, \\ = 0; & t < \dfrac{-T}{2} \text{ and } \dfrac{T}{2} < t. \end{array} \tag{A2.6}$$

The Fourier transform of the gating function is

$$G(s) = \frac{\sin(x\pi)}{x\pi} \qquad \text{(A2.7)}$$

where x is the ratio of input frequency to sampling frequency (Cox, 1978). Thus in order to generate spectral components of different frequency but equal amplitude, as our model requires, it is necessary to compensate for the relative attenuation imposed by sampling. The synthesis program included such compensation.

Additionally, it may be shown that the sampling procedure results in replications of the input spectrum at multiples of the sampling frequency. This effect is shown graphically in Figure A2.3. We note that the higher the sampling rate, the further apart will be the individual spectra. In order to prevent spectral overlap (aliasing), a sampling frequency of at least twice the highest input frequency must be employed; this is termed the Nyquist criterion.

The first replication of the signal (input) spectrum, can be shown to begin at the difference between the highest frequency of the signal and the sampling frequency. That is, the "worst case" is represented by the highest frequency to be synthesized. In the present study, this highest frequency was 2486 Hz. In order to be able to filter out replications of the signal spectrum, we employed a sampling rate of 10,000 amplitude values per second. That is, for our "worst case", replications of the noise-band began at 7514 Hz. Substituting these values in Eq. (A2.7) indicates that the level of the "first alias" is 10.5 dB below the level of the original component.

To further attenuate these spectral replications (aliases), we employed an 8-pole Butterworth low-pass filter (Rockland 1042F) with a cutoff set always to 1.4 times the highest frequency synthesized (i.e., 1.4 x 2486 = 3480).

Figure A2.3

Pictorial representation of the effects of sampling on stimulus spectrum. Striped bars represent original and first replicated spectrum. Solid curve represents the envelope of the *sync* function. A sampling rate of 10000 is assumed.

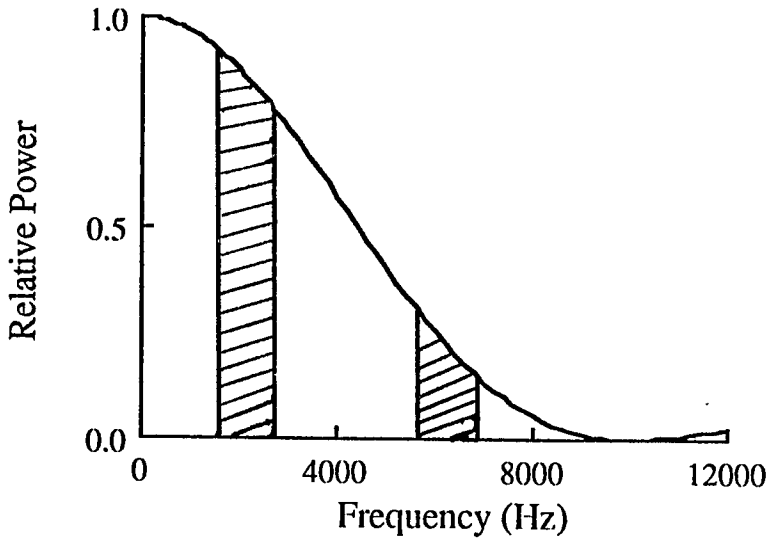
1.0
0.5
0.0
Relative Power
0
4000
8000
12000
Frequency (Hz)

The transfer of power of the Butterworth low-pass filter is given by the expression

$$\frac{P_{out}}{P_{in}} = \frac{1}{1+(f/f_c)^{16}}. \qquad \text{(A2.8)}$$

The attenuation at 7514 (the first "alias" frequency) is approximately -53 dB. Therefore the total attenuation of the first alias component was approximately 64 dB. Inasmuch as the first alias component represents our "worst case", the overall signal-to-alias power ratio is greater than 64 dB. The noise waveform was virtually unaffected by the anti-alias filter; its highest frequency component was attenuated less than 0.02 dB.

5.2.2.2 Quantization Error

Our amplitudes were to be limited to integer values in the range -2048, 2048 (i.e., based on a 12 bit binary representation). On the other hand, real noise amplitudes are continuously variable. This leads to "quantization error" (Gold and Raner, 1969). Such error, may be considered to be a uniform noise "floor", which was -83 dB relative to overall stimulus power (Lovell and Carterette, 1972).

5.2.3 The Synthesis Algorithm

5.2.3.1 Noise Bands

5.2.3.1.1 Sampling

Employing noise representation A2.1 and assuming unit sine wave amplitude, synthesis of each burst began by selecting a random starting phase angle for the lowest frequency component of that band. The Fortran program then calculated the value of the sine function (Taylor series expansion) for that angle. The attenuation of this lowest frequency due to sampling was determined, and the first instantaneous amplitude was multiplied by the inverse. This value was then stored in the first position of an array. The program next determined the increment in phase angle that would occur at the next sampling point (i.e., 100 microseconds later) and this was added to the starting

phase. Again, the value of the sine of this angle was determined, and again the sync function compensation was applied. This value was then stored in the second position of the array. The process was then repeated, storing the amplitude values sequentially in the array, until 1024 samples were collected. This, then represented the amplitudes of the low frequency component, sampled every 100 microsecond. The program then determined the frequency of the next higher component in such a manner that uniform frequency sampling would be obtained with at least $2WT$ components. A random starting phase was determined for this second component; this sinusoid was sampled every 100 microseconds as described above. The amplitude at each sampling point was added to that of the previous component. The process was continued until all components for the noise-band had been digitized. Figure A2.4 presents a flow-chart of the process for synthesizing noise-bands.

5.2.3.1.2 Scaling

Since the synthesis employed sine waves of unit amplitude, it was desirable to scale our stimuli, so that we would obtain the largest RMS voltage from our digital-to-analog conversion without "undue" clipping. The nature of Gaussian noise, as described earlier, is such that any amplitude value is possible. Since our 12-bit representation requires that the maximum amplitude value correspond to 4096/2, we decided to set the maximum equal to 4 times the RMS voltage (i.e., to have a crest factor of 4). It may be recalled that the variance of the amplitude-sampling distribution for a single component equals ½ (and that this also represents the average power). It follows then, that the variance of N independent components equals $N/2$, and that the standard deviation (RMS voltage) equals $\sqrt{N/2}$. Since we wished to limit peaks to 4 times the RMS voltage, and to utilize the full range of the D/A converter (12 bits), the program calculated the value of $2048/\sqrt{N/2}$, and multiplied the stored amplitudes at each sampling point by this value. Peaks which exceeded 2048 were set equal to 2048.

Figure A2.4

Flow chart of the (off-line) synthesis routine.

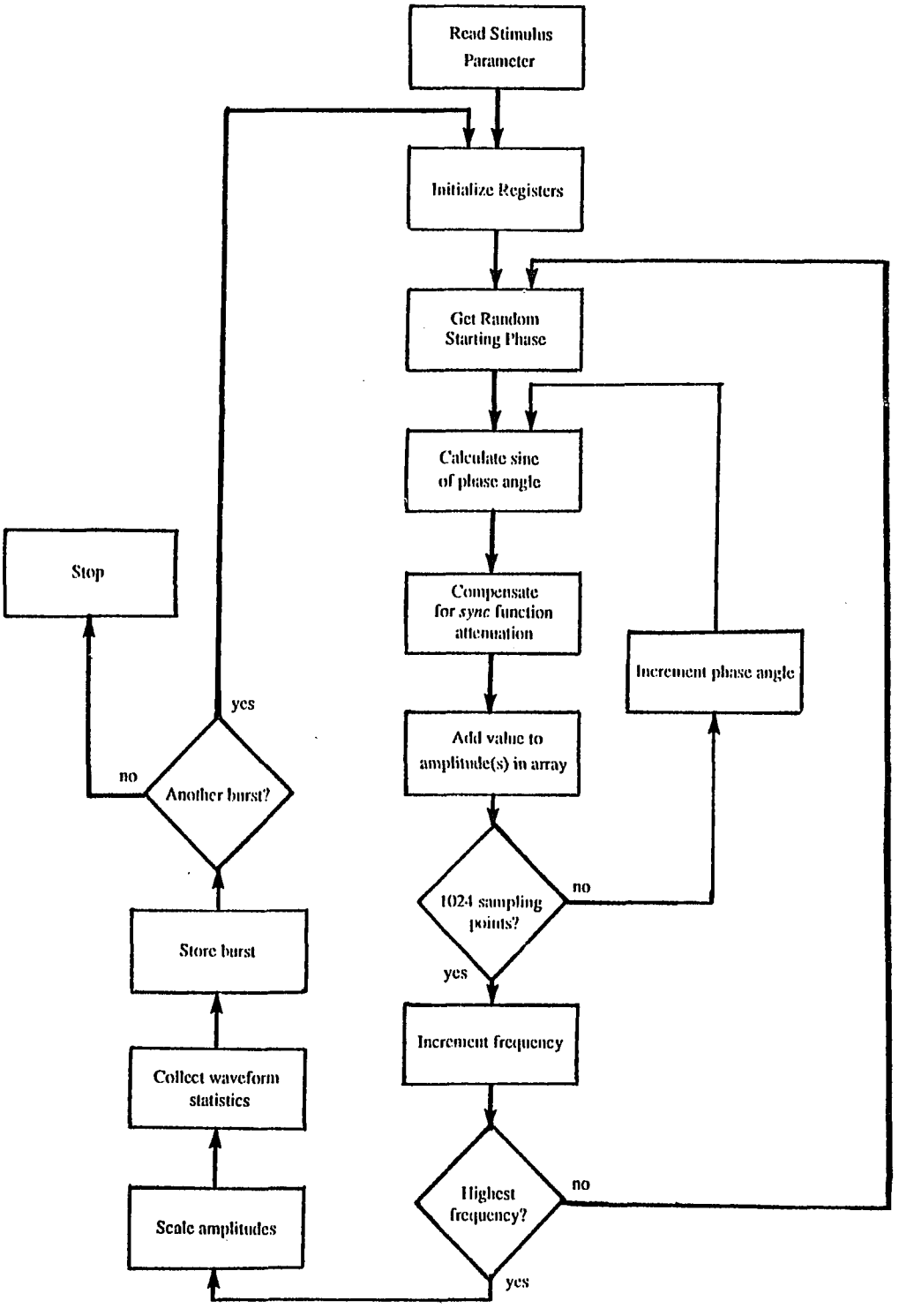
Read Stimulus Parameter
Initialize Registers
Get Random Starting Phase
Calculate sine of phase angle
Compensate for sync function attenuation
Add value to amplitude(s) in array
1024 sampling points?
no
yes
Increment phase angle
Increment frequency
Highest frequency?
no
yes
Scale amplitudes
Collect waveform statistics
Store burst
Another burst?
yes
no
Stop

The amplitude values were then truncated to integer form. This scaling procedure also afforded the opportunity to determine the frequency of peaks exceeding 4σ. Data on peaks, as well as other pertinent sample statistics were collected during synthesis, and are discussed in APPENDIX III.

After scaling of the noise-burst, its amplitude values were stored on disk (DEC RK05) and the synthesis procedure repeated for another burst of the same bandwidth.

5.2.3.2 Tonal Signals

The tonal signals employed in the present study were synthesized in a fashion similar to that for the noise-bursts except that; only a single frequency component was employed (f = 1500 Hz) which began at a positive-going zero-crossing.

5.2.4 Preparation of DECtapes

The outputs of the synthesis programs were amplitudes stored as ASCII coded decimal values in the range -2048, 2048. For on-line generation of the stimuli, it was necessary to convert these representations to a 12 bit 2's compliment binary form and to store these on DECtape. A program was developed for that conversion, and used to prepare the magnetic tapes. For each noise bandwidth, a separate tape was prepared, on which each burst was recorded sequentially in the order of synthesis. An additional tape was prepared for the tonal signals.

5.2.5 On-Line Generation of Stimuli

A program was written for on-line stimulus generation, stimulus sequencing, signal level control and data acquisition. For a given condition, each threshold determination began by transferring from DECtape to the computer's memory, the binary representation of two signal and two masker waveforms. At the start of each observation interval, the computer provided a pulse which was used to start a digital timing system (Iconix 6255/6010). The digital timing system controlled an electronic

switch (Grason-Stadler 1287-B) that was used to gate the stimuli. This arrangement provided synchronization of the switching action with the production of the synthetic waveforms. Timing was adjusted so that the onset of the envelope ramp coincided with the begining of the synthetic waveform. Timing was also adjusted so that the end of the envelope coincided with the end of the waveform. In the present study, 5 msec rise and fall-times were employed. Since the duration of the synthetic waveforms was always 102.4 msec, the envelope's decay began 97.4 msec after the start of each observation interval.

For each trial, new signal and masker waveforms were transferred from DECtape to the computer's memory. At the appropriate time, the first amplitude value of the masker was transferred from memory to the Digital-to-Analog converter (Adac 600-8ED) for the masker channel. Immediately afterwards the first amplitude value of the signal was transferred to the other D/A converter. Asynchrony between the masker and signal waveforms was approximately 5 microseconds. After 100 microseconds, the second pair of amplitude values was then transferred to the appropriate converters. The process was repeated for all subsequent pairs of amplitude values. The timing of this sequence was controlled by the computer's processor (crystal) clock; the necessary machine instructions included "dummy" steps. Figure A2.5 presents a flowchart of the stimulus production routine. Timing in all other parts of the program was controlled by the computer's real-time programmable clock.

5.2.6 Stimulus Sequencing

The time required for off-line synthesis varied directly with the number of components required. For bandwidths less than 792 Hz, 180 different noise samples were produced. For wider bandwidths, it was not practical to synthesize so many different bursts. Table A2.1 presents the number of components for each bandwidth, as well as the number of different noise-bursts synthesized.

Table A2.1

Number of components employed in the synthesis of noise bursts, and the number of different bursts generated.

Bandwidth (Hz)	Number of Components	Number of Bursts Generated
50	51	180
63	64	180
79	80	180
100	101	180
158	80	180
500	126	180
629	156	180
792	166	80
1000	251	100
1256	268	120
1581	337	60

Figure A2.5

Flow chart of the (on-line) stimulus generation routine.

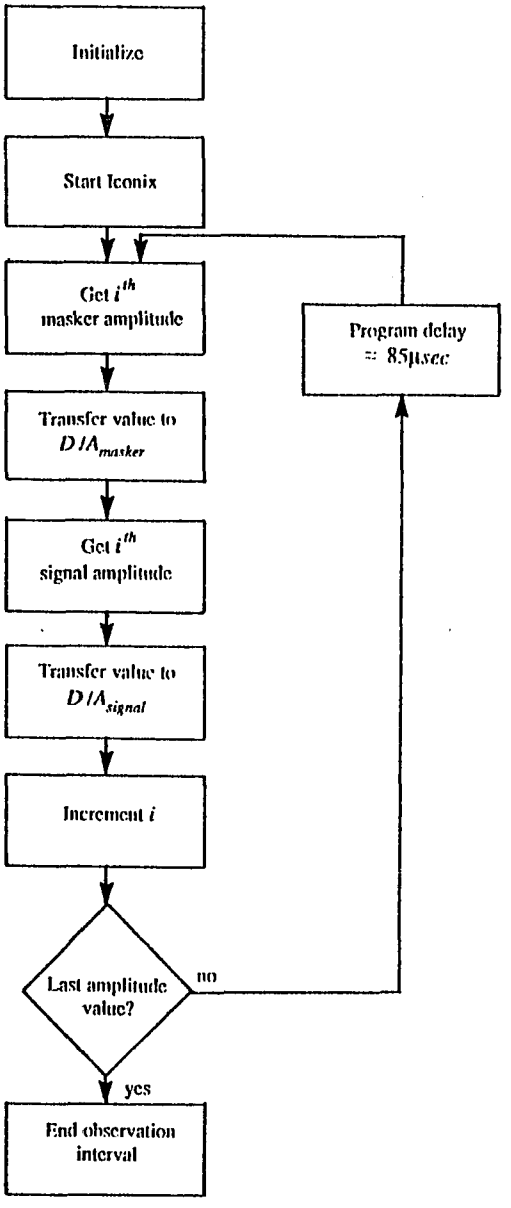
Initialize
Start Iconix
Get i^{th} masker amplitude
Transfer value to D/A_{masker}
Get i^{th} signal amplitude
Transfer value to D/A_{signal}
Increment i
Last amplitude value?
no
yes
End observation interval
Program delay = 85μsec

Since, the number of different samples of a given bandwidth was limited, it was arranged that the same combination of signal and masker waveforms would not be repeated during a particular threshold determination ("staircase"). This was accomplished as follows: The first trial of each threshold determination began with randomly selected samples of signal and masker. The stimuli were then presented in order of synthesis until the last sample on the DECtape was used. The order of stimuli was then reversed with the constraint that 5 masker and 3 signal samples were skipped. Reversing was repeated, if necessary, when the first stimulus on the DECtape was reached. Reversals occurred independently for signal and masker tapes. For example, when the signal and masker had different bandwidths, and each tape contained 180 samples, a "staircase" might begin with the first pair of bursts (no. 1). After 90 trials, the two ensembles of bursts were exhausted. On the 91^{st} trial, the first masker burst presented would be no. 175, while the first signal employed would be no. 177. This procedure of reversing-plus-skipping made it very unlikely that a given signal-masker combination would be repeated during the 400-500 trials (5 staircases) used to estimate each threshold.

5.2.7 Level Calibration

The D/A converters were strapped to produce +10 and, -10 volt outputs with inputs of 2048 and -2048, respectively. For our synthetic stimuli, the scaling procedure was such that the RMS voltage would be 2.5 volts. For the noise stimuli, this is so on average; any single noise burst might depart from this average. For all practical purposes, our tonal stimuli were unvarying. Since both tone bursts and noise bursts were 102.4 msec in duration, voltages could not be measured with a conventional voltmeter. For these reasons, a calibration tone was synthesized, whose duration could be as long as required, and whose RMS voltage equaled 2.5.

One cycle of a 1000 Hz waveform was sampled and scaled in a fashion similar to that for the other stimuli. In this case, 10 amplitude values were stored in the computer's memory. On command, the amplitude values were transferred to the D/A converters at the rate of one every 100 microseconds. By arranging that the last amplitude value (at 360 ° - 36 °) would be followed by the first, a continuous tone of 1000 Hz was produced. The measured voltages at the output of the anti-alias filters agreed within 0.2 dB with each other, and with the calculated value. This continuous tone was used for level calibration.

Since the scaling procedure (see section 3.1.2 above) resulted in equal overall levels at all bandwidths, noise spectral-density varied inversely with bandwidth. The attenuations required for equal spectral-densities were readily calculated and easily obtained.

5.2.8 Spectral analysis

5.2.8.1 Hum and Harmonic Distortion of Calibration Tone

A wave-analyzer (GR 1568-A) was used to measure hum and the distortion of the calibration tone at both the output of the anti-alias filters, and at a point in the circuit just before the subject's earphone. Table A2.2 presents the results of this analysis. To check the accuracy of the timing of the D/A conversions, the frequency of the calibration tone was measured with a frequency counter (HP 5300) and found to be 1000.0. Generated stimulus frequencies are accurate within .01%.

Table A2.2

Hum and distortion measurements of 1000-Hz calibration tone. Measurements were made after the anti-alias filter and also before delivery to the listener's earphone. Each measurement is referred to the level of the calibrating tone at that point in the circuit.

Frequency (Hz)	Level (dB re Fundamental)	
	After Anti-alias Filter	Before Earphone
60	-69	-72
120	<-75	<-75
180	-74	<-75
1000	0	0
2000	<-75	<-75
3000	<-75	<-75
4000	<-75	<-75
10000	<-75	<-75

Figure A2.6

Average spectrum of 128 samples of: a) 50 Hz wide synthetic noise b) 450 Hz wide synthetic noise c) 1500 Hz tone.

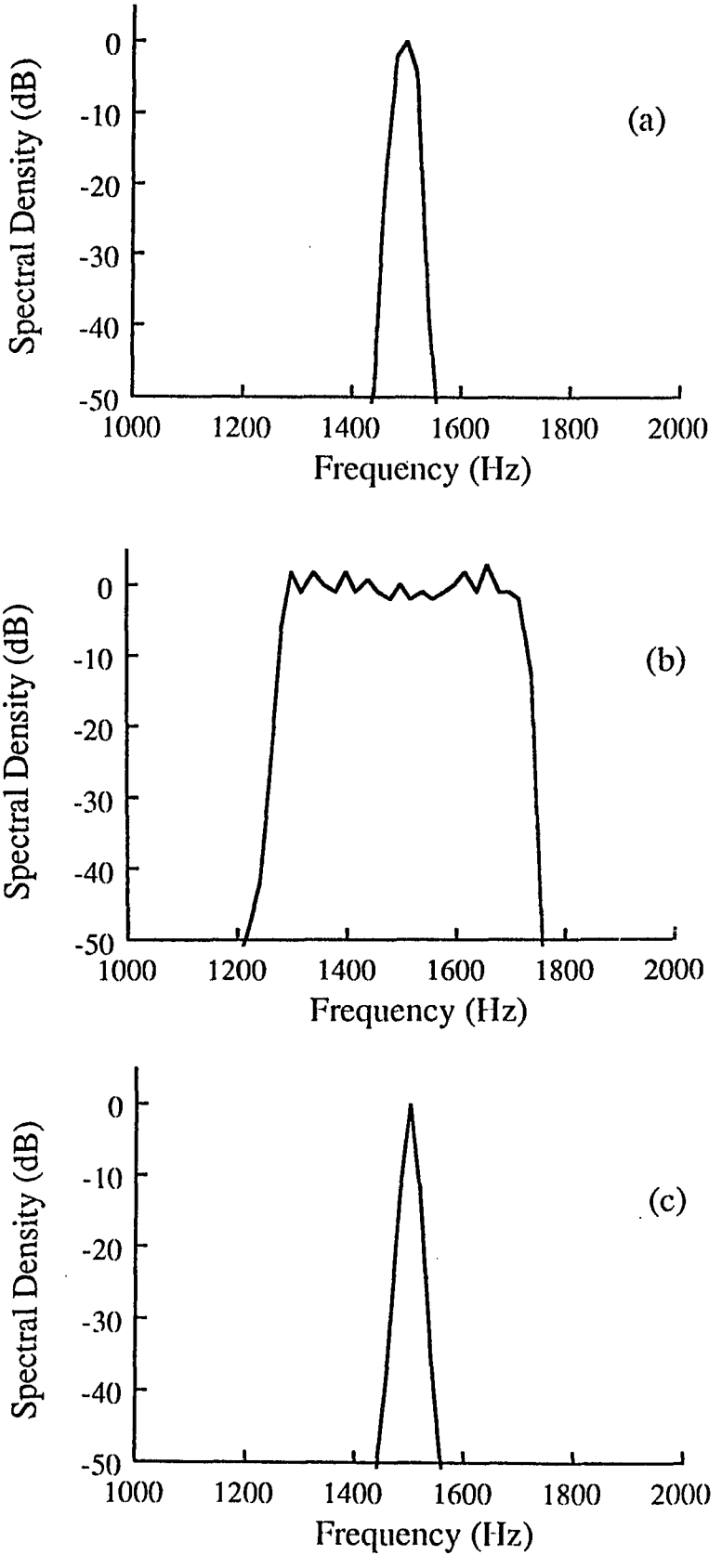
Spectral Density (dB)
0
-10
-20
-30
-40
-50
1000
1200
1400
1600
1800
2000
Frequency (Hz)
(a)
(b)
(c)

5.2.8.2 Spectrum of Noise Bursts

Figure A2.6 present the average spectra of 128 noise bursts whose bandwidths equals 50 and 450 Hz, respectively. These spectra were obtained with a Fast Fourier Transform spectral analyzer (HP 3582A) set to have a 100 msec time window with Hanning weighting. Measurements were made at the output of the anti-alias filters. It is evident that the average spectra are reasonably flat within the passbands. The rate of attenuation outside the passbands exceed 1.4 dB/Hz. This finite attenuation, is due to the duration of the analysis. This may be demonstrated by comparing the spectral envelope of a 1500 Hz tone, generated by a low distortion oscillator (HP 239A), to that of the noise bands. Figure A2.6c presents the spectrum of the tone obtained in the same fashion as those of the noise-bands. Clearly, the rates of off-frequency attenuation are similar. Had the time window of analysis been increased, the spectral envelope of the tone would have been sharper.

5.3 APPENDIX III -- Evaluation of Synthetic Noise

During the off-line synthesis and prior to scaling, we collected data on the mean amplitude, the average number of zero crossings, the number of amplitudes exceeding four times the standard deviation, and the average "energy" and variability of "energy" for each bandwidth of noise. In this section, we present predictions of these statistical properties based on the noise model and we compare these to the data obtained during synthesis. As a final evaluation, we compare noise-intensity discrimination of our synthetic stimuli, to that obtained with thermally generated stimuli.

5.3.1 Amplitude Characteristics

5.3.1.1 Mean Amplitude

The model of noise requires that the amplitude distribution of $n(t)$ be symmetric about zero (i.e., there are no DC components). Since this symmetry is independent of N, the expected value of $n(t)$ always equals zero. Table A3.1 presents obtained mean (instantaneous) amplitudes for our synthetic noise-bandwidths. These means are based on at least 60,000 amplitude values. In all cases, there is close agreement with expectation.

5.3.1.2 Mean Number of Zero-Crossings

Rice (1954) has shown that for rectangular bands of noise the expected rate of zeros is

$$2\left[\frac{1}{3}\cdot\frac{f_b{}^3-f_a{}^3}{W}\right]^{\frac{1}{2}} \qquad \text{(A3.1)}$$

where f_a and f_b are the low and high frequency bandlimits, respectively. The expected number of zero crossings, is given by the product of rate and duration. Table A3.2 presents, the expectations, together with the observed mean numbers of zero

Table A3.1

Mean amplitude of noise waveforms synthesized at each bandwidth.

Bandwidth (Hz)	Mean Amplitude
50	0.000
63	-0.001
79	0.000
100	0.000
158	-0.002
500	0.001
629	0.000
792	0.002
1000	0.002
1256	-0.003
1581	0.000

Table A3.2

Expected and observed number of zero crossings and deviates exceeding 4 σ for each bandwidth of synthetic noise.

Bandwidth (Hz)	Number of Zeros		Number of deviates beyond 4 σ	
	Expected	Obtained	Expected	Obtained
50	307	306	11.8	1
63	307	307	11.8	1
79	307	307	11.8	3
100	307	306	11.8	6
158	308	307	11.8	2
500	313	312	11.8	8
629	316	313	11.8	10
792	321	320	10.5	8
1000	328	326	6.5	6
1256	341	338	7.9	10
1581	360	355	3.9	4

crossings for each bandwidth of synthetic noise. Good agreement is evident.

5.3.1.3 Frequency of Extreme Amplitudes

It may be recalled that as part of our amplitude-scaling procedure (see APPENDIX II), we had occasion to record the occurrences of amplitudes more deviant than four times the population's standard deviation (σ). Since the noise described by the model has an amplitude distribution that is Gaussian, we may readily compare predicted frequency of occurrence (4σ deviations) to those obtained during synthesis. Table A3.2 presents this comparison. In all cases there were fewer extreme deviates than predicted. There is a tendency for the frequency of extreme deviates to come closer to expectation with increases in the the number of components (N) employed in the synthesis. This suggests, that the discrepancy from the model is due to the finite sampling (in the frequency domain) of our noise-bursts. Since the kurtosis of our amplitude distributions approximated that of the Gaussian (see APPENDIX II), we may conclude that our amplitude distributions are well described by a normal law except in the extreme tail-regions (see also, Slack 1946). It may be worth noting here that peak-limiting of a thermal source will also distort the frequency of extreme amplitudes.

5.3.2 The 'Energy' of Synthesized Noise Bursts

5.3.2.1 Mean 'Energy'

For the discrete temporal representation of our noise waveforms, we may define the "energy" of each burst as being proportional to the sum of the squared amplitudes. It may be recalled that the average power of a unit sine wave is ½. It follows, then, that the average power of N such sine waves added without regard to phase is $N/2$. Average energy is given by the product of average power and duration. Table A3.3 presents, as a function of bandwidth, the expected and observed mean energies. The two sets of values are in close agreement.

Table A3.3

Comparison of expected and obtained 'energies' and relative variabilities of 'energy' for each noise bandwidth.

Bandwidth (Hz)	'Energy'		Mean-to-Sigma Ratio of 'Energy'	
	Expected	Obtained	Expected	Obtained
50	26112.0	25009.0	2.26	2.66
63	32768.0	31843.9	2.54	2.91
79	40960.0	39553.1	2.84	3.34
100	51712.0	52294.9	3.20	3.61
158	40960.0	39941.9	4.02	4.67
500	64512.0	64928.3	7.16	9.48
629	76800.0	77423.2	8.03	11.26
792	84992.0	86185.3	9.01	12.55
1000	128512.0	129764.7	10.12	12.56
1256	137216.0	139014.1	11.34	18.37
1581	172544.0	175272.2	12.74	17.14

5.3.2.2 Relative Variability of 'Energy'

The relative variability (σ/M) of the distribution of energy, of a noise with a rectangular spectrum is given by

$$\frac{1}{\sqrt{WT}}. \tag{A3.2}$$

We determined relative variabilities of energy for our noise-bursts; these are presented along with the expected values in Table A3.3. We note that our synthetic waveforms exhibit less energy fluctuation than is predicted by the model. The change of relative variability with bandwidth is consistent with the predictions of the model. Ratios of obtained-to- expected relative variabilities range from 1.16 to 1.62. Insofar as performance in a noise-intensity discrimination task is determined by relative energy fluctuations, the reduced relative variability would result 0.6 to 2.0 dB improvement in threshold depending on bandwidth. Since our amplitude distributions are in agreement with the model everywhere except in the matter of extreme amplitude excursions, this departure might be responsible for the reduced energy variability.

5.3.3 Discrimination of Intensity with Synthetic and Thermal Noises

Noise-intensity discrimination with thermally generated stimuli was compared to that obtained with our synthetic waveforms. Stimulus spectrum was matched by bandlimiting the 1581 Hz wide synthetic noise to bandwidth of 500 Hz with two Rockland (852) filters connected in cascade (attenuation rate of 96 dB/octave). The thermal source (GR, 1390-B) was bandlimited in the same manner. All other stimulus parameters were the same as in the main study. Figure A3.1 presents a block diagram of the modifications of the apparatus employed in this condition.

Figure A3.1

Block diagram of apparatus used for the experiment comparing intensity discrimination with thermal and synthetic noise. Noises were bandlimited to 500 Hz.

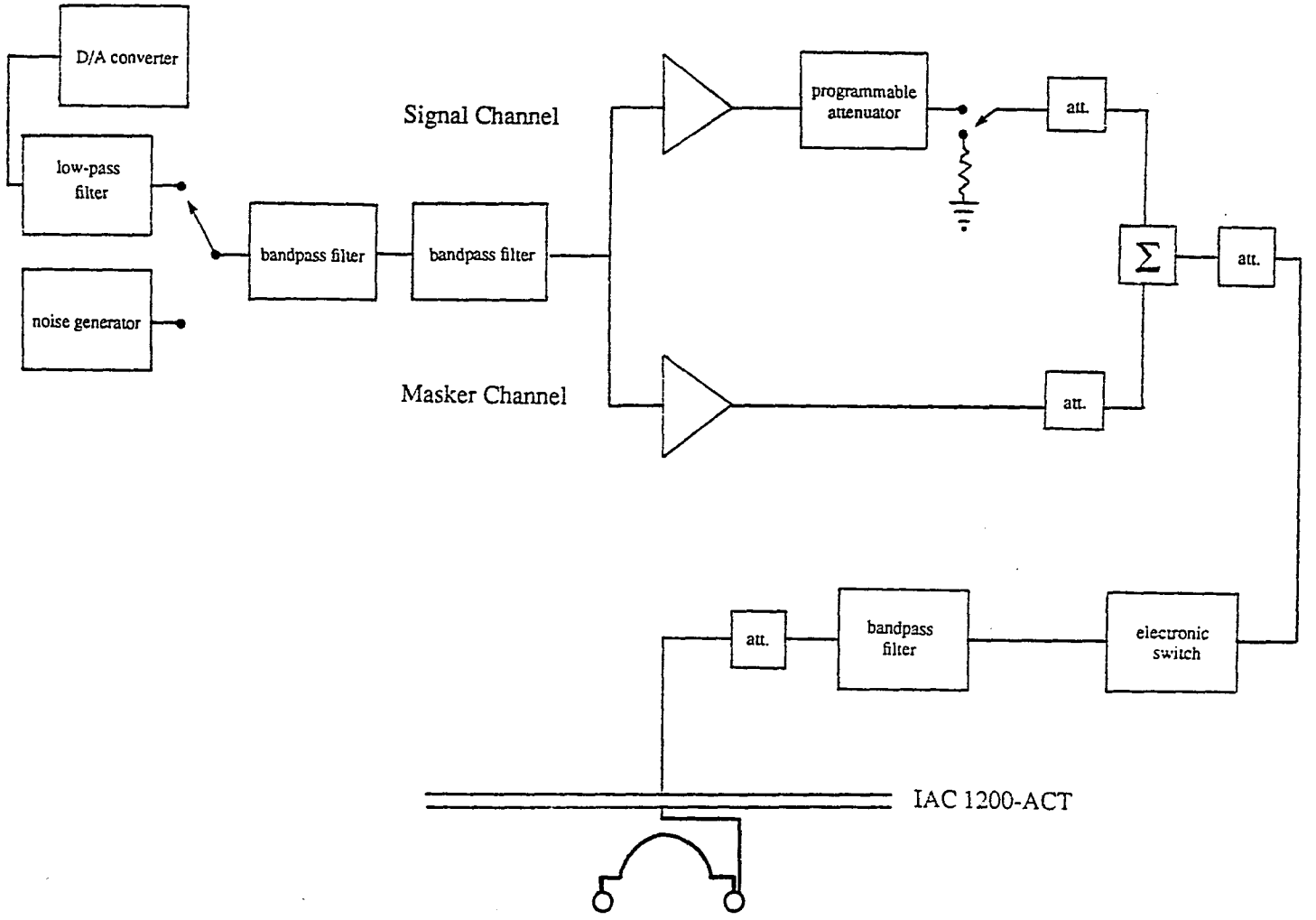
D/A converter
low-pass filter
noise generator
bandpass filter
bandpass filter
Signal Channel
Masker Channel
programmable attenuator
att.
att.
Σ
att.
att.
bandpass filter
electronic switch
IAC 1200-ACT

Table A3.4

Difference thresholds ($10 \log S_0/N_0$) obtained with synthetic and with thermal noise. $W_s = W_n = 500$ Hz.

Noise Source		Listener		
	N_0	JA	RB	Mean
Thermal	8	-2.1	-2.1	-2.1
	38	-3.0	-2.4	-2.7
	Mean	-2.5	-2.3	-2.4
Synthetic	8	-2.2	-3.9	-2.9
	38	-1.9	-2.6	-2.3
	Mean	-2.1	-3.3	-2.6

Thresholds were determined in the same fashion as in the main study with the following modifications: First, The output of the bandlimiting filter was split and led to two channels -- one for the signal, the other for the masker. Hence, the signal waveform was always added in phase with the masker. Second, thresholds were determined with a 3 dB step-size.

Presented in Table A3.4 are the mean thresholds obtained (expressed as 10 log S_0/N_0) with each of the noise sources tested, for each of the observers. Clearly all values agree within experimental error, both within and between observers. We may therefore conclude, that our synthetic noise reproduces those characteristics that are important for intensity-discrimination.

5.4 APPENDIX IV -- Procedure for fitting lines to Fletcher plots

Since we assume that the detection mechanism includes internal filtering, we expect that a plot of signal threshold (in dB) as a function of masker bandwidth (W_n) would be of the form:

$$\begin{aligned} signal\ threshold &= m \log W_n + B; & W_n &< W_c, \\ signal\ threshold &= m \log W_c + B; & W_n &\geq W_c. \end{aligned} \qquad \text{(A4.1)}$$

The data may be fitted with two line segments -- an ascending limb in the region where $W_n < W_c$, and a second limb of zero slope where $W_n \geq W_c$. The "breakpoint" at W_c provides an estimate of the bandwidth of the detection process. To estimate the slope and intercept of the first limb and W_c the data must be partitioned into two sets; thresholds at bandwidths above and thresholds at bandwidths below W_c. To do this we employed an iterative least-squares procedure (Bogartz, 1968). Essentially, the procedure begins by partitioning the data such that the two narrowest masker bands are assumed to be narrower than W_c. A least-squares regression solution is then obtained for the initial line segment. The total residual sum of squared deviations around both lines is computed. In order to maximize this value, the procedure employed all individual threshold determinations. The data are then repartitioned such that the initial line is now fitted to the three narrowest bandwidths. Again total residual sum of squared deviations is computed around the two new lines. Repartitioning continues until all but the widest masker bandwidth (5000 Hz) is included in the initial line segment.

The partitioning which minimizes the total residual sum of squares is regarded as the best and the least-squares solution for that initial segment is taken as the best

estimate of the slope (m) and intercept (B). The "critical" bandwidth (W_c) is the bandwidth at which the two lines intersect.

6. *REFERENCES*

Bendat, J.S. and Piersol, A.G. (1971). *Random Data: Analysis and Measurement Procedures* (Wiley-Interscience, New York).

Bernstein, R.S. and Baruch, E. (1977). Unpublished experiments.

de Boer, E. (1962). "Note on the critical bandwidth," Journal of the Acoustical Society of America, 34, 985-986.

de Boer, E. (1965). "Detection function for noise bands," Paper F26 in proceedings of the 5th International Congress on Acoustics, Liege.

de Boer, E. (1966). "Intensity discrimination of fluctuating signals," Journal of the Acoustical Society of America, 40, 552-560.

Bogartz, R.S. (1968). "A least-squares method for fitting intercepting line segments to a set of data points," Psychological Bulletin, 70, 749-755.

Bos, C.E. and de Boer, E. (1966). "Masking and discrimination," Journal of the Acoustical Society of America, 39, 708-715.

van den Brink, G. (1964). "Detection of tone pulses of various durations in noises of various bandwidths," Journal of the Acoustical Society of America, 36, 1206-1211

Campbell, R.A. (1964). "Masker level and noise-signal detection," Journal of the Acoustical Society of America, 36, 708-715.

Cox, R.G. (1978). "Window functions for spectrum analysis," Hewlett Packard Journal, September, 10-11.

Durlach, N.I. (1963). "Equalization and cancellation theory of binaural masking-level differences," Journal of the Acoustical Society of America, 35, 1206-1218.

Fletcher, H. (1940). "Auditory Patterns," Reviews of Modern Physics 12, 47-65.

Gold, B. and Raner, C. (1966). *Digital Processing of Signals* (McGraw-Hill, New York).

Green, D.M. (1960). "Auditory detection of a noise signal," Journal of the Acoustical Society of America, 32, 121-131.

Green, D.M. (1966). "Signal detection analysis of equalization and cancellation model," Journal of the Acoustical Society of America, 40, 833-838.

Green, D.M. and McGill, W.J. (1970). "On the equivalence of detection probabilities and well-known statistical quantities," Psychological Review, 77, 294-301.

Green, D.M. and Swets, J.A. (1974). *Signal Detection Theory and Psychophysics* (Kreiger, New York).

Greenwood, D.D. (1961). "Auditory masking and the critical band," Journal of the Acoustical Society of America, 33, 484-502.

Houtgast, T. (1972). "Psychophysical evidence for lateral inhibition in hearing," Journal of the Acoustical Society of America, 51, 1885-1894.

Houtgast, T. (1977). "Auditory-filter characteristics derived from direct-masking data and pulsation-threshold data with a rippled-noise masker," Journal of the Acoustical Society of America, 62, 409-415.

Hamilton, P.M. (1957). "Noise masked thresholds as a function of tonal duration and masking noise bandwidth," Journal of the Acoustical Society of America, 29, 506-511.

Hawkins, J.E. and Stevens, S.S. (1950). "The masking of pure tones and of speech by white noise," Journal of the Acoustical Society of America, 22, 6-13.

Henning, G.B. (1967). "A model for auditory discrimination and detection Journal of the Acoustical Society of America, 42, 1325-1334.

Henning, G.B. (1973). "Effect of interaural phase on frequency and amplitude discrimination," Journal of the Acoustical Society of America, 54, 1160-1178.

Leshowitz, B. and Wightman, F.L. (1971). " On-frequency masking with continuous sinusoids," Journal of the Acoustical Society of America, 41, 1180-1190.

Lovel, J.D. and Carterette, E.C. (1972). "Digital generation of acoustic stimuli," Behavior Research Methods and Instrumentation 4, 151-155.

Mathews, M.V. and Pfafflin, S.M. (1965). "Effects of filter type on energy-detection models for auditory signal detection," Journal of the Acoustical Society of America, 38, 1055-1056.

McGill, W.J. (1967). "Neural counting mechanism and energy detection in audition," Journal of Mathematical Psychology 4, 351-376.

Moschetto, C.F. (1978). "On the measurement of noise-intensity discrimination by up-down psychophysical methods," Doctoral dissertation, City University of New York, New York.

Moschetto, C.F., Bernstein, R.S. and Raab, D.H. (1980). "Noise intensity discrimination as measured by up-down psychophysical methods," The Journal of Auditory Research 20, 113-118.

Miller, G. (1947). "Sensitivity to changes in the intensity of white noise and its relation to masking and loudness," Journal of the Acoustical Society of America, 19, 609-615.

Moore, B.C.J. (1975). "Mechanisms of masking," Journal of the Acoustical Society of America, 57,391-399.

Moore, B.C.J. and Raab, D.H. (1975). "Intensity discrimination for noise bursts in the presence of a continuous, bandstop background: Effects of level, width of bandstop and duration," Journal of the Acoustical Society of America, 57, 400-405.

Patterson, R.D. (1976). "Auditory filter shapes derived with noise stimuli," Journal of the Acoustical Society of America, 59, 640-654.

Patterson, R.D. and Henning, G.B. (1977). "Stimulus variability and auditory filter shape," Journal of the Acoustical Society of America, 62, 649-664.

Pfafflin, S.M. and Mathews, M.V. (1962). "Energy detection model for monaural auditory detection," Journal of the Acoustical Society of America, 34, 1842-1853.

Pfafflin, S.M. and Mathews, M.V. (1966). "Detection of auditory signals in reproducible noise," Journal of the Acoustical Society of America, 39, 340-345.

Raab, D.H. and Bernstein, R.S. (1979). "Effects of masker level on detection of a tone in pseudorandom noise," Journal of the Acoustical Society of America, 66, 299-301.

Raab, D.H. and Goldberg, I.A. (1975). "Auditory intensity discrimination with bursts of reproducible noise," Journal of the Acoustical Society of America, 57, 437-447.

Rice, S.O. (1954). Mathematical Analysis of Random Noise in N. Wax (ed.) *Noise and Stochastic Proceses* (Dover press, New York).

Schacknow, P.N. and Raab, D.H. (1976). "Noise-intensity discrimination: effects of bandwidth conditions and mode of masker presentation," Journal of the Acoustical Society of America, 60, 893-905.

Schaeffer, T.H., Gales, R.S., Shewmaker, C.A. and Thompson, P.O. (1950). "The frequency selectivity of the ear as determined by masking experiments," Journal of the Acoustical Society of America, 22, 490-496.

Scharf, B. (1970. Critical Bands in J.V. Tobias (ed.) *Foundations of Modern Auditory Theory* (Academic Press, New York).

Sever, J.C. and Small, A.M. (1979). "Binaural critical masking," Journal of the Acoustical Society of America, 1343-1350.

Small, A.M., Bacon, W.E. and Fozard, J.L. (1959). "Intensive differential thresholds for octave-band noise," Journal of the Acoustical Society of America, 31, 508-510.

Slack, M. (1946). "The probability distribution of sinusoidal oscillations combined in random phase," Journal of the Institute of Electrical Engineers, 93, 76-86.

Spiegel, M.F. (1979). "The range of spectral intergration," Journal of the Acoustical Society of America, 66, 1356-1363.

Spiegel, M.F. (1981). "Thresholds for tones in maskers of various bandwidths as a function of signal frequency," Journal of the Acoustical Society of America," 69, 791-795.

Swets, J.A., Green, D.M. and Tanner, W.P., Jr. (1962). "On the width of critical bands," Journal of the Acoustical Society of America, 34, 108-113.

Watson, C.S. (1964). "Measurment of individual stimuli in a signal detection task," Journal of the Acoustical Society of America, 36 (S), 1042.

Weber, D.L. (1978). "Suppression and critical bands," Journal of the Acoustical Society of America, 64, 141-150.

Weir, C.C., Schlauch, R.S. and Norton, S.J. (1984). "The relations among critical ratios, critical bands and intensity difference limen in man," Journal of the Acoustical Society of America, 76, 1051-1056.

Zwicker, E., Flottorp,G. and Stevens, S.S. (1957). "Critical bandwidth in loudness summation," Journal of the Acoustical Society of America, 29, 548-557.